



HAL
open science

Evidences for a Paleocene marine incursion in southern Amazonia (Madre de Dios Sub-Andean Zone, Peru)

M. Louterbach, M. Roddaz, J. Bailleul, P.-O. Antoine, S. Adnet, J.H. Kim, E. van Soelen, F. Parra, J. Gérard, Y. Calderon, et al.

► To cite this version:

M. Louterbach, M. Roddaz, J. Bailleul, P.-O. Antoine, S. Adnet, et al.. Evidences for a Paleocene marine incursion in southern Amazonia (Madre de Dios Sub-Andean Zone, Peru). *Palaeogeography, Palaeoclimatology, Palaeoecology*, 2014, 414, pp.451 - 471. 10.1016/j.palaeo.2014.09.027 . hal-04166498

HAL Id: hal-04166498

<https://hal.science/hal-04166498>

Submitted on 26 Jul 2023

HAL is a multi-disciplinary open access archive for the deposit and dissemination of scientific research documents, whether they are published or not. The documents may come from teaching and research institutions in France or abroad, or from public or private research centers.

L'archive ouverte pluridisciplinaire **HAL**, est destinée au dépôt et à la diffusion de documents scientifiques de niveau recherche, publiés ou non, émanant des établissements d'enseignement et de recherche français ou étrangers, des laboratoires publics ou privés.

See discussions, stats, and author profiles for this publication at: <https://www.researchgate.net/publication/267155176>

Evidences for a Paleocene marine incursion in Southern Amazonia (Madre de Dios Sub-Andean Zone, Peru)

Article in Palaeogeography Palaeoclimatology Palaeoecology · November 2014

DOI: 10.1016/j.palaeo.2014.09.027

CITATIONS

17

READS

925

13 authors, including:



Mélanie Louterbach

Repsol

25 PUBLICATIONS 113 CITATIONS

[SEE PROFILE](#)



Martin Roddaz

Paul Sabatier University - Toulouse III

98 PUBLICATIONS 2,246 CITATIONS

[SEE PROFILE](#)



Julien Bailleul

UniLaSalle (Beauvais)

32 PUBLICATIONS 136 CITATIONS

[SEE PROFILE](#)



Pierre-Olivier Antoine

Université de Montpellier

277 PUBLICATIONS 3,829 CITATIONS

[SEE PROFILE](#)

Some of the authors of this publication are also working on these related projects:



Geoarcheology [View project](#)



Seismic stratigraphy and stratigraphic modeling of offshore trench-slope basins, active Hikurangi margin, North Island, New Zealand [View project](#)

Evidences for a Paleocene marine incursion in southern Amazonia (Madre de Dios Sub-Andean Zone, Peru)

M. Louterbach^{a,b,c,*}, M. Roddaz^a, J. Bailleul^b, P.-O. Antoine^d, S. Adnet^c, J.H. Kim^e, E. van Soelen^e, F. Parra^a, J. Gérard^c, Y. Calderon^f, C. Gagnaison^b, J.S. Sinninghe Damsté^e, P. Baby^a

^a Géosciences-Environnement Toulouse, Université de Toulouse, UPS (SVT-OMP), LMTG, CNRS, IRD, 14 Avenue Édouard Belin, F-31400 Toulouse, France

^b Bassins-Réservoirs-Ressources, Institut Polytechnique Lasalle Beauvais, Département Géosciences, 19 rue Pierre Waguet, BP 30313, F-60026 Beauvais Cedex, France

^c REPSOL Exploración S.A., Calle Mendez Alvaro 44, 28045 Madrid, Spain

^d Institut des Sciences de l'Évolution (ISE-M, UMR – CNRS 5554), c.c. 64, Université Montpellier 2, Place Eugène Bataillon, F-34095 Montpellier Cedex 05, France

^e Royal Netherlands Institute for Sea Research (NIOZ), Department of Marine Organic Biogeochemistry, Den Burg, Texel, The Netherlands

^f PERUPETRO S.A., Luis Aldana 320, San Borja, Lima, Peru

ARTICLE INFO

Article history:

Received 4 October 2013

Received in revised form 19 September 2014

Accepted 26 September 2014

Available online xxxx

Keywords:

Paleogene

Marine incursion

Amazonian foreland basin

Tidal deposits

Madre de Dios basin

Peru

ABSTRACT

This article presents new biostratigraphic dating, facies analysis, organic geochemical data and Nd–Sr isotopic provenance from five outcrops of southern Amazonia (MD-85, MD-177 MD-184, MD-255 and MD-256) to document for the first time the presence of a shallow marine incursion in the Paleocene of southern Amazonia basin. The co-occurrence of a selachian assemblage encompassing *Potobatis* sp., *Ouledia* sp., and *Pristidae* indet. with the ostracod *Protobuntonia* sp. and the charophytes *Peckichara* cf. *varians meridionalis*, *Platychara perlata*, and *Feistiella* cf. *gildemeisteri* suggests a Paleocene age for the studied deposits (most likely Thanetian but potentially Danian). Fifteen facies have been recognized and have been grouped into three facies assemblages. Facies association A corresponds to the sedimentary filling of a tide-influenced meandering channel formed in the fluvial–tidal transition zone. Facies association B is related to more distal tidal-flats, little channelized tidal inlets and saltmarsh deposits. Facies association C corresponds to a stressed shallow marine environment such as a bay or a lagoon. The $\delta^{13}\text{C}_{\text{TOC}}$ value (-23.4‰) of MD-184 is enriched in ^{13}C compared to the other samples suggesting the presence of substantial amounts of marine organic matter in MD-184. The $\delta^{13}\text{C}_{\text{TOC}}$ values of samples from other outcrops (-27.3 to -29.8‰) indicate a mixed organic matter origin, from terrestrial to brackish environments. The analyzed sediments have similar Nd–Sr isotopic compositions as those of the Cenozoic sediments of the Altiplano ($\epsilon\text{Nd}(0)$ values from -6.2 to -10.7 and $^{87}\text{Sr}/^{86}\text{Sr}$ compositions from 0.712024 to 0.719026) indicating a similar volcanic source. This multidisciplinary dataset documents the presence of a tide-dominated estuary sourced by the proto-Western Cordillera debouching into a shallow marine bay during Paleocene times. This transgression might be explained by subsidence created in response to the proto-Western Cordillera loading. Similar to Miocene marine incursions affecting the Pebas megawetland, Paleogene marine incursions in the Amazonian foreland basin associated with Andean uplift may have played a role in the Neotropical biodiversity dynamics in favoring biogeographical isolation and promoting allopatric speciation for terrestrial organisms.

1. Introduction

The Amazon basin is the world's largest Cenozoic fluvial basin with an actual drainage area of $5.8 \times 10^6 \text{ km}^2$ and a depositional area of approximately 2.5 to $3 \times 10^6 \text{ km}^2$. The Amazon rainforest, with an area of about $5.6 \times 10^6 \text{ km}^2$, is the largest rainforest ecosystem, representing nearly 50% of the total tropical rainforest area on Earth. The Amazon rainforest plays a significant role in global climate, the carbon cycle and biodiversity and is the most species-rich terrestrial ecosystem in the world. However, the timing of the origin and evolutionary causes

of this diversity are still highly debated. A recent synthesis by Hoorn et al. (2010) has highlighted the complex links between Andean mountain building, climate variability and biodiversity development throughout Cenozoic times in the Amazonian basin. In particular the occurrence of inland seaway is important not only in promoting biogeographical isolation and allopatric speciation but also in controlling the precipitation rates in the Amazon basin (Jeffery et al., 2012). Consequently, determining the number, timing and duration of Cenozoic marine incursions recorded in Amazonian basin is fundamental not only for reconstructing paleo-Amazonian landscapes and ecosystems through time but also for understanding the close relationships between Andean mountain building and the Cenozoic climate and biotic evolution of South America.

* Corresponding author.

E-mail address: melanie.louterbach@repsol.com (M. Louterbach).

Several marine incursions have already been described in the Cenozoic sedimentary record of the Amazonian foreland basins (Roddaz et al., 2010). For instance, the existence and persistence of the early to middle Miocene Pebas megawetland system in northern Amazonia are thought to have promoted the high biodiversity of the Amazon rainforest (for a review, see Hoorn et al. (2010) and references therein). However, the extent of this Pebas system and the number of marine incursions that have occurred are still under debate (Campbell et al., 2006; Hovikoski et al., 2007; Hoorn et al., 2010) mainly because of poor stratigraphic dating and the lack of regional data integration. In comparison, few studies document Paleogene marine incursions in the Amazonian basin. For instance, there is some evidence of a marine incursion during Eocene to Oligocene times in Colombia (Santos et al., 2008), Ecuador (Christophoul et al., 2002) and northern Peru (Hermoza et al., 2005b), but no data exist for earlier marine incursions.

In this study, new biostratigraphical, sedimentological and geochemical data are presented to highlight a Paleocene marine incursion in southern Peru, Madre de Dios basin. A new paleo-depositional model for these coastal deposits is also proposed. Finally, the paleogeography and paleo-extension of this shallow marine incursion are discussed.

2. Geological background

2.1. Paleocene sedimentary record in the Amazonian foreland basins

In nearly all the Central Andean sedimentary basins, late Eocene to early Oligocene times are marked by a widespread sedimentary hiatus (Mpodozis and Allmendinger, 1993; Marocco et al., 1995) corresponding to a major tectonic phase primarily called Incaic 1 phase (Noble et al., 1990; Jaillard, 1996; Hermoza, 2004). However, there are some localities in northern and Central Andean foreland basins where Paleocene strata have been preserved and can be described (Figs. 1 and 2).

In central Colombia, the Cuervos Formation is late Paleocene in age (Jaramillo and Dilcher, 2000, 2001) and its sedimentary rocks correspond to mudstones deposited in a distal alluvial to coastal plain environment, in a foredeep position (Cooper et al., 1995; Parra et al., 2009). In the Putumayo basin of southern Colombia, the Rumiyaco Formation is barren of fossils and then remains poorly constrained but it is assumed that it is early Paleocene in age. The Rumiyaco Formation unconformably overlays the Cretaceous series and builds up a sedimentary wedge onlapping onto older strata and disappearing toward the east of the basin. The formation is characterized by possibly marine-related to mostly continental fine-grained deposits in the western part of the Putumayo basin and evolves eastward into continental sandstones (Bejarano, 1991; Casero, 1997; Córdoba et al., 1997; Londoño et al., 2012). In the Ecuadorian Oriente basin, Paleocene strata dated by charophytes (Faucher and Savoyat, 1973) are represented by the deposits of the fluvial Tena Formation. Various studies demonstrated that sediments from Tena Formation are derived from the Eastern Cordillera of Ecuador (Ruiz et al., 2004, 2007; Martin-Gombojav and Winkler, 2008).

In Peru, Paleocene strata are very scarce and are only identified in the eastern border of the Altiplano (Vilquechico Group and Lower Muñani Formation), in the Cusco–Sicuaní area (Puquin Formation) or in the present-day foreland basin (Yahuarango or Huayabamba Formations) (Sigé et al., 2004; Gelfo and Sigé, 2011). These strata generally consist of reddish fine-grained continental deposits and are defined as the Red bed Formation (Naeser et al., 1991; Jaillard, 1993a; Hermoza et al., 2005b). The Lower Muñani Formation is dated between 55.9 and 53.4 Ma by mammalian biostratigraphy and by magnetostratigraphy (Cande and Kent, 1992; Sigé et al., 2004). The Yahuarango (Huallaga and Marañon basins) and Huayabamba (Madre de Dios and Beni basins) formations are poorly constrained. Only a few charophytes have been documented and provide a Paleocene age (Gutiérrez, 1982) for these fluvial deposits (Fig. 2).

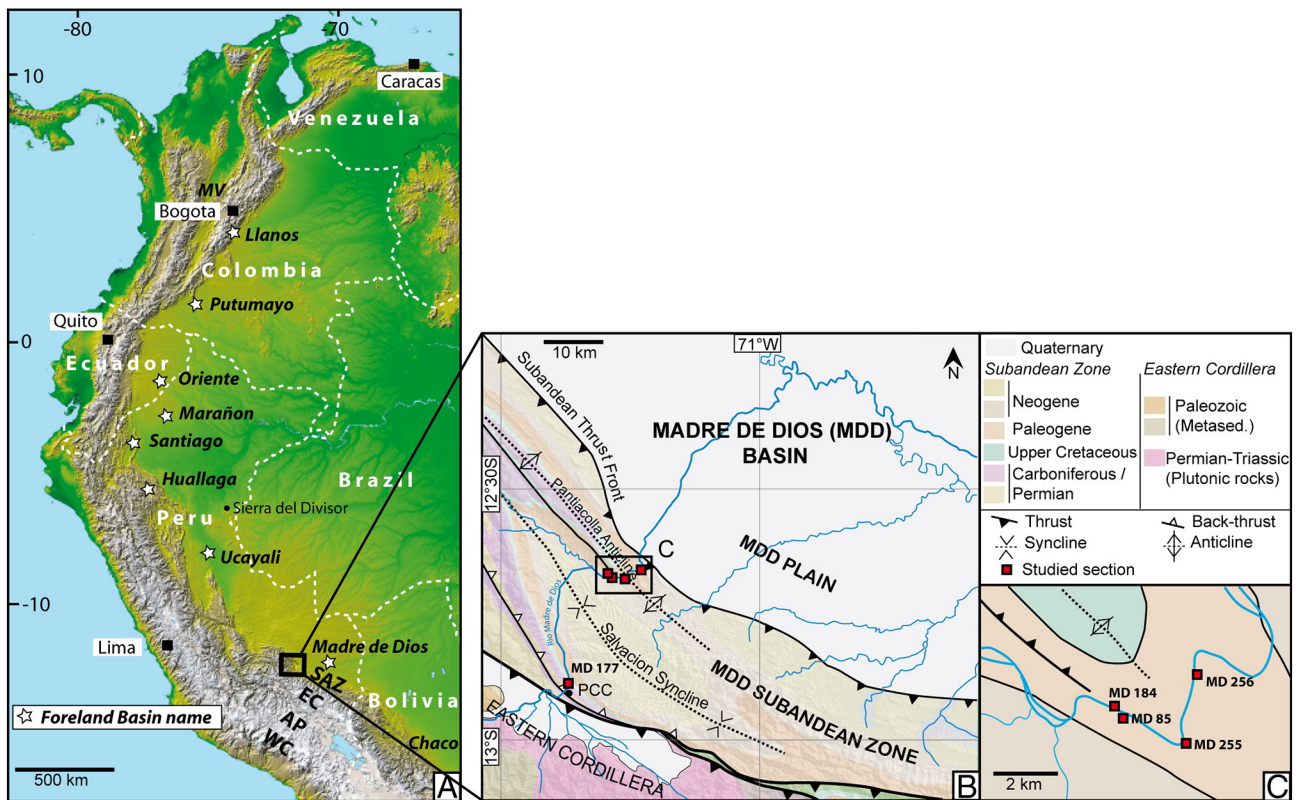


Fig. 1. A) White stars display Amazonian foreland basin location (northern Andes and part of Central Andes). B) Simplified geological and structural map of the study area. Red squares display the location of the outcrops used for this study. PCC = Pongo de Coñeq Canyon. C) Zoom of Pantiacolla anticline area, and location of the outcrops. (For interpretation of the references to color in this figure legend, the reader is referred to the web version of this article.)

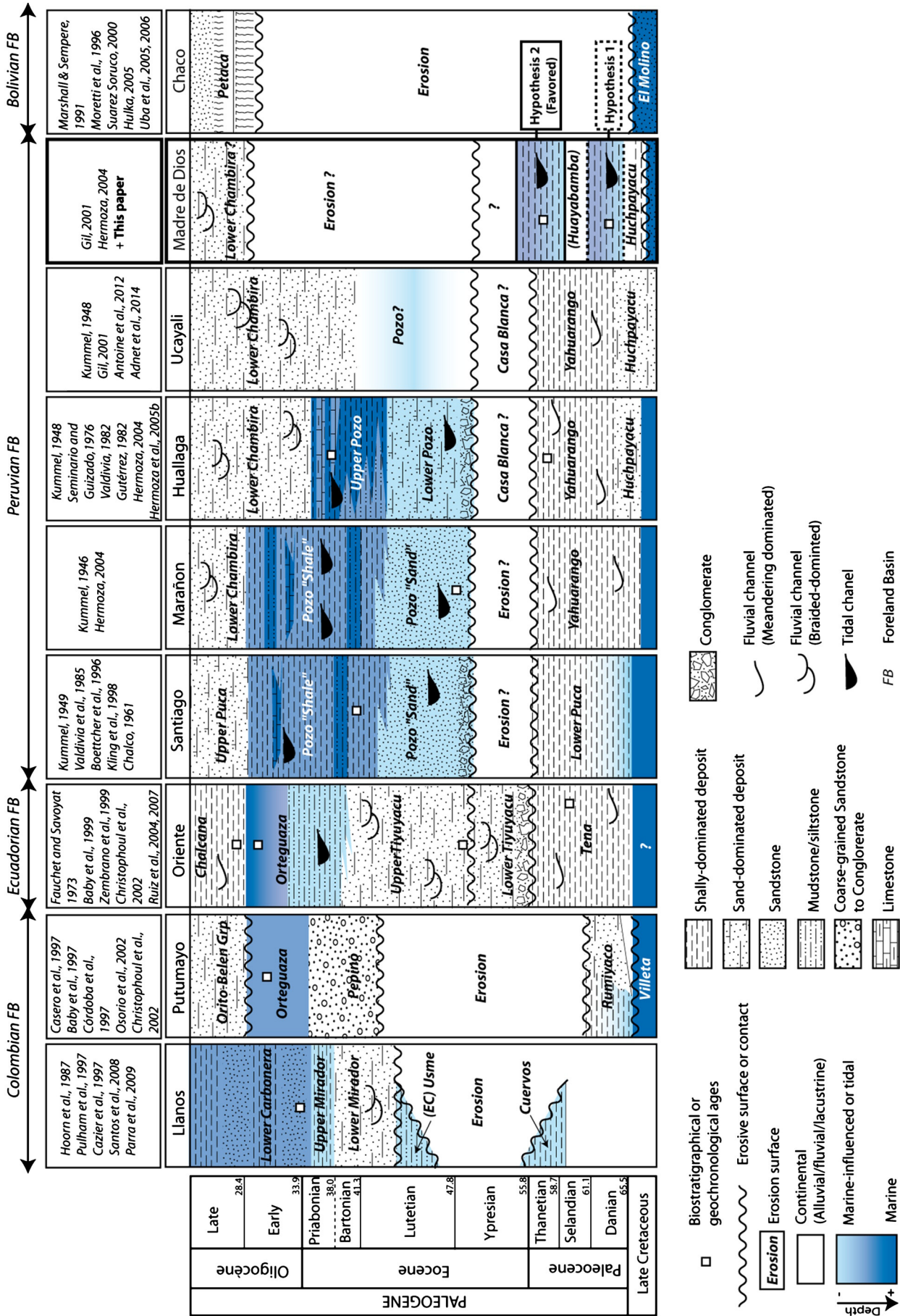


Fig. 2. Stratigraphic correlation chart for Paleogene strata between Amazonian foreland basins from Colombia to northern Bolivia. Shallow marine deposits are colored in blue. Important biostratigraphical or geochronological references are displayed by white squares. EC = Eastern Cordillera.

Table 1
Distribution and relative abundance of fossil content of biostratigraphical interest in Paleocene localities from the Upper Madre de Dios Sub-Andean Zone, Southeastern Peru. Ost = Ostracoda; (r) = potentially reworked; (+) = close ally, Relative abundance is denoted by the number of "+" (ranging from + up to +++++).

Locality	Vertebrata				Ost.				Foraminifera				Charophyta			
	<i>Ouledia</i> sp.	<i>Potobatis</i> sp.	? <i>Dasyatidae</i> sp. 1	? <i>Dasyatidae</i> sp. 2	<i>Pristidae</i> indet.	<i>Pycnodontidae</i> indet.	<i>Serrasalminae</i> indet.	<i>Protobuntonia</i> sp.	<i>Karreriella</i> <i>conversa</i>	<i>Reophax</i> sp.	<i>Bathysiphon</i> sp.	<i>Rhabdammina</i> sp.	<i>Peckichara</i> cf. <i>meridionalis</i>	<i>Platychara</i> <i>perlata</i> ?	<i>Feistiella</i> cf. <i>gildemeisteri</i>	
MD-85	+	(r)					(+)	+								
MD-177	+++					++	++									
MD-184	+++					++	++									
MD-255	+					+										

In Bolivia, Paleocene strata are virtually absent in the Amazonian foreland basin (Roddaz et al., 2010) (Fig. 2). Paleocene deposits documented in the Eastern Cordillera of southern Bolivia correspond to the mostly continental Santa Lucía and Cayara Formations, Danian and Thanetian in age, respectively (Marshall et al., 1997; DeCelles and Horton, 2003). However, a typically marine stingray (*Potobatis semperi*) was recently recognized within a marly horizon at the top of the Danian Santa Lucía Formation (Cappetta and Gayet, 2013).

2.2. Stratigraphy and structure of the Madre de Dios basin

The Madre de Dios basin is part of the southern Amazonian foreland basin system (Roddaz et al., 2005a). The Madre de Dios foreland basin is located northeastward to the Eastern Cordillera (EC) of southern Peru and can be subdivided into the Sub-Andean Zone (SAZ) and the Madre de Dios plain tectonomorphic units (Fig. 1-B) (Gil, 2001; Hermoza, 2004). The SAZ is characterized by both sedimentary filling and active deformation. In the SAZ, propagation of deformation towards the Madre de Dios plain is controlled by the development of deep duplexes, whose shortening is accommodated in surface by imbricates and by the Sub-Andean thrust front. The Sub-Andean thrust front corresponds to the eastern border of the SAZ and is responsible for transportation of a piggy-back basin, which outcrops as a large syncline called Salvación syncline in the study area (Fig. 1-B). The deformed and still active SAZ only corresponds to the internal (western) part of Madre de Dios foreland basin. The external (eastern) part of the basin is situated east to the Sub-Andean thrust front and corresponds to the non-deformed part of the system, the Madre de Dios plain. In this study, we will only focus on outcropping strata from the Salvación syncline, in the SAZ of Madre de Dios basin.

Upper Cretaceous to Cenozoic strata in Salvación piggy-back basin consist of +/- 4500 m of an alternance of marine, tide-influenced and fluvial deposits (Gil, 2001; Hermoza, 2004). Because of the very scarce outcrops, fauna and palynomorph material available in the studied area, the general chronostratigraphy of this succession is quite difficult to assess and many interrogations subsist for the Cretaceous–Paleogene interval (Gil, 2001; Hermoza, 2004), while Miocene deposits are much better constrained in terms of biochronology and chronostratigraphy (Marivaux et al., 2012; Antoine et al., 2012, 2013, Submitted for publication). Paleogene strata in the Salvación series and more broadly in the Madre de Dios basin are supposed to correspond to the fluvial Huayabamba or the Red bed Formation.

3. Methodology

In the Madre de Dios basin, Paleogene deposits crop out along the Alto Madre de Dios River between the Pongo de Coñeq Canyon and the Pantiacolla anticline, which correspond to the verticalized flanks of the Salvación syncline (Fig. 1-B). This paper focuses on five selected exposures in cutbanks along the Alto Madre de Dios River. The section includes MD-177, MD-255, MD-256, MD-85 and MD-184 outcrops (Fig. 1-B and C). Their precise locations are given in the online Supplementary Table A. The five concerned localities yield similar micro- and macrofossils (foraminifers, charophytes, molluscs, ostracods, as well as chondrichthyan and actinopterygian fishes), which allows us to consider them as being time equivalent (Table 1 and Fig. 3). Fifteen sedimentary facies are characterized on the basis of their lithologies, their physical and biogenic sedimentary structures, their palynological and paleontological contents, and their geometry (Table 2). For limestone layers of MD-184, standard microfacies descriptions have also been realized. Each of these fifteen facies is interpreted in terms of depositional processes and related depositional environment. On the basis of these interpretations and with regard to the geometrical relationships between the facies, three facies associations are proposed (Table 2).

In order to determine the nature of the organic matter (terrestrial versus marine), we analyzed four samples for $\delta^{13}\text{C}_{\text{TOC}}$ content

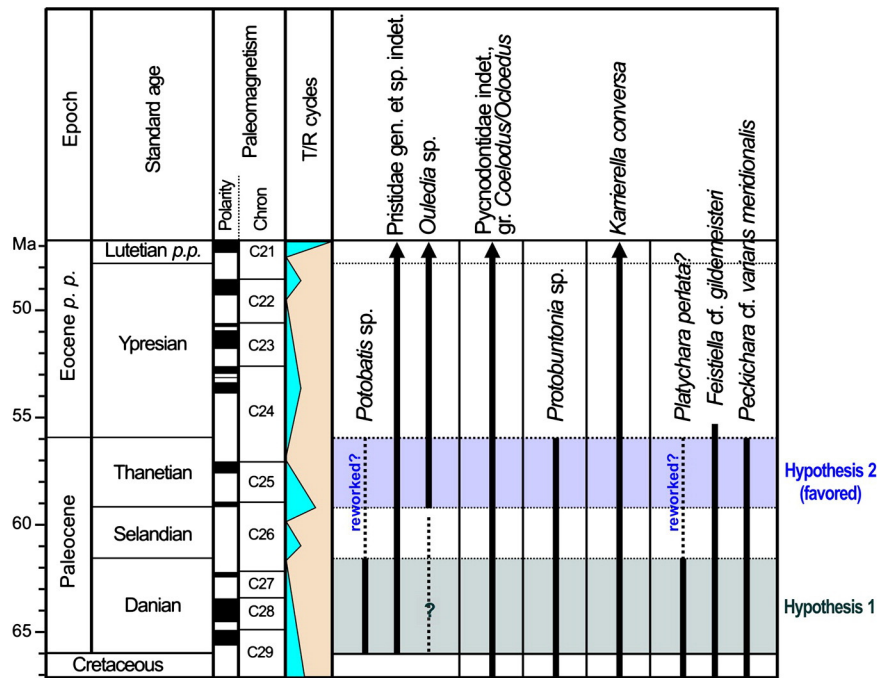


Fig. 3. Stratigraphical range of biostratigraphical markers in Paleocene localities from the Upper Madre de Dios SAZ, Southeastern Peru. T/R = Transgressive/regressive cycles, according to Vandenberghe et al. (2012). Based on data from Gradstein et al. (1988), Musacchio (1990); Gayet et al. (1993); Jaillard (1993a); Sigé et al. (2004); Gelfo et al. (2009); Gelfo and Sigé (2011); Morsi et al. (2011); Cappetta (2012); Gonella et al. (2012); Cappetta and Gayet (2013); Woodburne et al. (2014).

(Table 3) at the NIOZ Institute, Netherlands. The $\delta^{13}\text{C}_{\text{TOC}}$ of higher plants that use the Calvin–Benson cycle of carbon fixation (i.e. so-called C_3 plants) ranges from -29.3 to -25.5% , with an average value of about -27% (e.g. Tyson, 1995). The typical marine $\delta^{13}\text{C}_{\text{TOC}}$ values are in the range of -18 to -22% (e.g. Meyers, 1997). Additional geochemical rock-eval analysis (for sample MD 184) has also been carried out by Repsol Exploration S.A.

Four selected samples of mudstones from outcrops MD-177, MD-85, MD-184 and MD-255 were measured at the University of Toulouse for their Nd–Sr isotopic compositions, providing sedimentary provenance information (Table 4). Aliquots containing about 1000 ng of Sr and Nd were loaded onto the ion-exchange columns. Sr and Nd were separated using the Sr-SPEC, TRU-SPEC and LN-SPEC resins (Eichrom®). Nd–Sr isotopic ratios were measured using a Finnigan Mat 261 thermal ionization mass spectrometer in dynamic mode following Viers et al. (2008). The measured $^{143}\text{Nd}/^{144}\text{Nd}$ ratios are presented as the fractional deviation in parts per 10^4 (units) from $^{143}\text{Nd}/^{144}\text{Nd}$ in a Chondritic Uniform Reservoir (CHUR) as measured at the present-day:

$$\varepsilon\text{Nd}(0) = \left[\left(\frac{^{143}\text{Nd}}{^{144}\text{Nd}} \right)_s / I_{\text{CHUR}}(0) - 1 \right] * 10^4$$

where $(^{143}\text{Nd}/^{144}\text{Nd})_s$ is the present-day ratio measured in the sample, and $I_{\text{CHUR}}(0)$ is the $^{143}\text{Nd}/^{144}\text{Nd}$ in the CHUR reference reservoir at the present ($I_{\text{CHUR}}(0) = 0.512638$; Jacobsen and Wasserburg, 1980).

4. Results

4.1. New biostratigraphical and paleoenvironmental constraints from fossil assemblage

4.1.1. Biostratigraphy

The fossil content of stratigraphic interest recovered in the studied sections is detailed in Table 1 and Fig. 3. The concerned material includes vertebrates (chondrichthyans and actinopterygians), ostracods, benthonic foraminifers, and charophytes. Being only recognized at genus, family level, or above, the molluscs found in MD-177, MD-184,

and MD-85 are of no use in terms of biostratigraphy (Table 1). Accordingly, MD-177 and MD-184 yielded unidentified Charophyta and Ostracoda.

The dominant taxon among vertebrate remains in the concerned deposits is the batoid *Ouledia* sp. (MD-177; MD-184; MD-85; see Table 1 and Fig. 3 for biostratigraphical result details and Fig. 4C–D, I–J for an illustration of the key stratigraphic markers). This fossil genus of butterfly rays (gymnurids) is well-known in tropical coastal deposits from Africa and Asia, ranging from the Thanetian up to the Priabonian (Cappetta, 2012). In MD-184, *Ouledia* is found in association with a pristid sawfish. Pristids are a cosmopolitan family restricted to Cenozoic marine and estuarine localities at world scale (i.e., Danian and onward; Cappetta, 2012). In MD-85, *Ouledia* sp. (mainly represented by worn teeth) co-occurs with *Potobatis* sp. (Fig. 4G–H), a dasyatoid stingray so far endemic to Danian marine levels from the top of the El Molino Fm., Bolivia (Cappetta and Gayet, 2013). However, in MD-85, the prismatic teeth referred to as *Potobatis* sp. are eroded and might have been reworked, which would concur to consider the Danian epoch as a floor age for MD-85. The vertebrate assemblages also include dozens of teeth of an unidentified pycnodontid bony fish (MD-177, MD-184; Fig. 4E–F), distinct from but potentially allied to *?Ocloedus toncoensis* (Maastrichtian–Danian of South America; Gonella et al., 2012). Pycnodontids are well represented in Mesozoic and early Paleogene localities, before the family gets extinct during the middle Eocene (Gayet et al., 1993; Poyato-Ariza and Wenz, 2002).

Microfossils of high biostratigraphical interest were recovered in MD-255 and MD-85. The agglutinated benthonic foraminifer *Karreriella conversa* (Eggerellidae), found in MD-255, has an Upper Cretaceous–Lutetian range (Fig. 2; Gradstein et al., 1988; Valchev, 2007). The best constrained locality is MD-85, with a diversified charophyte flora (17 specimens of *Peckichara cf. varians meridionalis*; 10 specimens of *Platychara perlata?*; 15 specimens of *Feistiella cf. gildemeisteri*), the ostracod *Protobuntonia* sp., and benthonic foraminifers (*Reophax* sp., *Bathysiphon* sp., and *Rhabdammina* sp.). The ostracod *Protobuntonia* ranges from the Coniacian up to the Thanetian epoch (Morsi et al., 2011); the fragile and delicate valves referred to this taxon in MD-85 are complete (i.e., not likely to be transported or reworked). The

Table 2

Descriptions and interpretations of sedimentary facies. FA = Facies association.

Outcrops	FA	Code	Facies description	Thickness	Physical sedimentary structures	Bioturbation	Observations	Microfacies and biostratigraphy	Depositional environment
MD 255	Facies association A	A1	Tangential cross-bedded fine- to medium-grained sandstone	20 cm to 120 cm	Massive/large scale cross-bedding with reactivation surfaces in rhythmic bundles/ripples/planar lamination. Lag deposit possible at the base with millimetric to centimetric mud clasts. Millimetric mud drapes.	<i>Arenicolites</i> , <i>Dactiloides</i> (?) at the top	Occasional bidirectionality + rhythmicity		Compound dune/tidal dune of channel infill Fluvio-tidal transition
MD 255		A2	Oblique Heterolithic strata with climbing rippled cross-stratification	1 to 1.20 m	Flaser-bedding with asymmetrical ripples + mud drapes/wavy or planar bedding. Coarsening-up patterns.	Highly bioturbated	Current direction orthogonal to dipping + rhythmicity		Lower part of tidal influenced point bar (IHS)
MD 255		A3	Oblique Heterolithic strata with tangential cross-bedding	>60 cm	Sandy beds (20–40 cm-thick) with tangential cross-bedding and planar lamination at the base + mud drapes/muddy to silty beds (2 to 5 cm)	Bioturbated	Current direction orthogonal to dipping + rhythmicity + bidir.		Upper part of tidal influenced point bar (IHS)
MD 255		A4	Mudstone to siltstone, occasional rippled fine-grained sandstone	2 m, sandy layers: 10 cm	Planar stratification, ripples and climbing ripples in the silty and sandy layers	Roots traces at the top. Bioturbated		Marine + terrestrial (Table 1)	Channel abandonment + floodplain (crevasse splay)
MD 256/MD 85b	Facies association B	B1	Fine- to medium-grained sandstone	1 to 1.50 m	Massive, lag deposits possible at the base, sigmoid bedding (heights of set: 45 cm). Climbing ripples, trough cross-bedding at the top. FU general setting			Marine (Table 1)	Inlet tidal channel fill/ estuarine tidal bar Tide-dominated environment
MD 256		B2	Red mudstone	20 m	Gypsum nodules at the top	Bioturbated, roots traces			Supratidal saltmarshes
MD 256		B3	Siltstone & mudstone	0.50 to 4 m	Scattered lenticular bedding (with carbonaceous sand) or centimetric fine-grained sandstone.	Bioturbated		Marine (Table 1)	Intertidal mud flats
MD 256		B4	Highly burrowed sandstone/siltstone & heterolithic sandstone	1 to 5 m	Mud drapes, wavy and lenticular bedding. Fluid escape structures	Highly Bioturbated	Occasional bidirectionality		Intertidal to subtidal mixed to sandy flats
MD 256		B5	Rippled fine-grained sandstone	20 to 30 cm	Ripples				Top of sand flats (subtidal?)
MD 184/MD 85/MD 177	Facies association C	C1	Violet-reddish carbonaceous mudstone to siltstone with centimetric fine-grained sandy layers + thin carbonaceous layers	50 cm to >2 m	Ripples and climbing ripples within sandy layers			Marine (Table 1)	Confined marine environment with some flood events Bay/shallow marine
MD 184/MD 85/MD 177		C2	Bioturbated Facies C1	80 cm to 1 m	Common sandy/carbonaceous nodules, possible gypsum nodules,	Root traces, Bioturbation			Paleosol developed on emerged shallow marine deposits (C1)
MD 184		C3	Sand nodules breccia with muddy to silty matrix	15 to 50 cm	Sand nodules in a muddy matrix			(Table 1)	Episodic channel flow
MD 184/MD 85		C4	Alternation of marl/limestone	10 to 25 cm	Desiccation cracks at the top. Frequent carbonate nodules	Root traces at the top, burrows		Shallow marine: Oysters, fish vertebrae, annelids, ostracods, gasteropods.	Confined intertidal to palustre environment
MD 184		C5	Stromatholitic limestone	25 to 80 cm	Desiccation cracks at the top			Shallow marine: Stromatholith, annelids, ostracods	Confined and stressed marine environment, Intertidal
MD 184		C6	<i>Ostrea</i> limestone	10 to 25 cm	Desiccation cracks at the top	Root traces at the top, burrows		Shallow marine: Blue algae, Fish coprolith, ostracods, oysters	Confined marine environment, intertidal/infralitoral sup

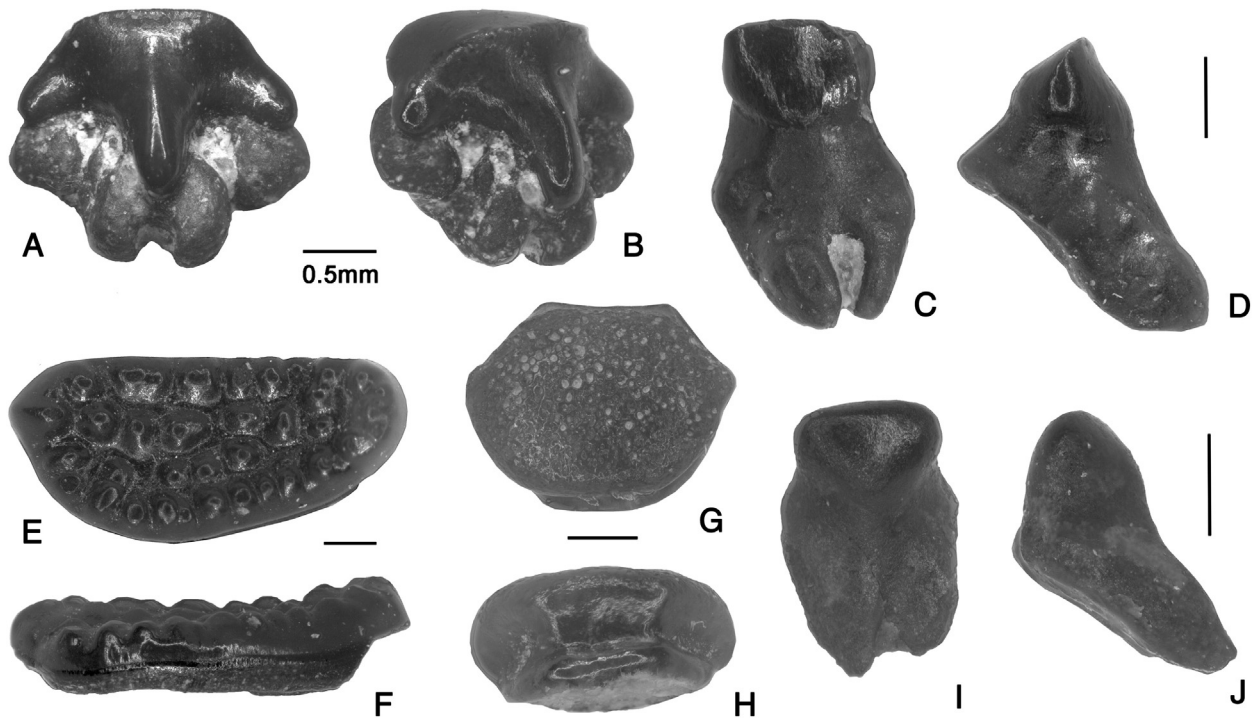


Fig. 4. Isolated teeth of marine-brackish fishes recovered from Paleocene MD-184 (A–F) and MD-85 (G–J) localities of the Upper Madre de Dios Sub-Andean Zone, Southeastern Peru. A–B: Pristidae gen. and sp. indet. (MD-184) oral tooth, A. lingual view, B. intermediate view. C–D: *Ouledia* sp. (MD-184) oral tooth, C. lingual view, D. lateral view. E–F: Pycnodontidae indet. (MD-184) palatine tooth, E. occlusal view, F. lateral view. G–H: *Potobatis* sp. (MD-85) fragmentary oral tooth, G. occlusal view, H. lingual view of crown (root lacking). I–J: *Ouledia* sp. (MD-85) worn oral tooth, I. lingual view, J. lateral view. Scale bar = 0.5 mm.

highlighted by thin mud drapes and generally present the same dip direction. However, some foresets can dip in the opposite direction. Facies A1 ends with an undulate rippled surface with heights of 1 to 2.5 cm and wavelengths of 15 to 20 cm, showing ichnofabrics *Arenicolites* and possible *Dactiloides* (Fig. 6-B and C) (Gérard and Bromley, 2008). Facies A1 corresponds to the coarsest deposits described in the area.

Facies A2 (total thickness of 1 to 1.20 m) consists of slightly oblique heterolithic strata (Fig. 6-F) overlying Facies A1 after a sharp transition (Fig. 5-B). Massive fine-grained sandstones or flaser bedding with asymmetrical climbing ripples highlighted by frequent mud drapes (15 to 30 cm thick) (Fig. 6-E) alternates with wavy bedding or planar muddy lamination in fine-grained sandstones (10 to 20 cm) (Fig. 6-G). The distribution of the thin planar mud drapes observed within the fine-grained sandstones of the wavy bedding often displays a rhythmic pattern, with intervals of inframillimetric sandstone beds evolving gradually to millimetric and then centimetric thicker sandy beds suggesting coarsening-up cycles (Fig. 6-G and F). Mud accumulation can be 1 mm to 1 cm thick. Horizontal and to a lesser extent vertical undetermined burrows are occasionally present.

Facies A3 also corresponds to slightly oblique heterolithic strata (total thickness > 60 cm). In comparison with Facies A2, Facies A3 is coarser as it is made up of thicker sandy beds (20 to 40 cm thick) intercalated with thin muddy to silty beds (2 to 5 cm thick). Fine-grained sandstones present tangential cross-bedding with planar laminations at their base representing their bottomset (Fig. 6-D). Rare asymmetrical ripples in the opposite direction can also be observed at the top of the tangential laminations. These sandstones are also heterolithic as almost all the sandy tangential and planar laminae are highlighted by thin mud drapes. Regular changing thicknesses of millimetric to centimetric sandy layers and inframillimetric to millimetric muddy layers suggest a rhythmic pattern (Fig. 6-D). Facies A1 and A3 are both made up of tangential cross-bedding in fine-grained sandstones, but differences with Facies A1 result in: 1) the scale of the structures (Facies A1 is made up of larger-scale cross-bedding compared to Facies A3), 2) the general geometry of the

bodies (Facies A1 corresponds to the laterally filling of a channelized body whereas Facies A2 corresponds to more tabular deposits) and 3) the texture and internal organization of the sediments (more finer texture and more heterolithic and rhythmic patterns for Facies A1).

Strata from both Facies A2 and A3 present an oblique pattern, prograding from the south-eastern channel margin towards the north-western margin of the channel (Fig. 5-A and B).

Facies A4 corresponds to siltstone layers (2 m thick) intercalated with fine-grained sandstone layers (10 cm thick). These sandstones present a sharp contact with the underlying siltstones and show climbing-ripple structures. Siltstones evolve upwards into mudstones (>2 m thick), where root traces develop at the top of the section. Rare benthic foraminifer *Karreriella conversa* can be preserved in this facies.

4.2.1.2. Interpretation. Stacked channel geometries as observed at MD-255 are common in fluvial and tidal settings. In both cases channels are erosive at their base and can be composed of fining- and thinning-up strata evolving gradually upwards into shaly strata. These shales can correspond to either fluvial floodplain or tidal flat deposits depending on the depositional environment.

The massive or cross-bedded fine- to medium-grained sandstones with basal mud clasts above erosional surfaces (Facies A1) could represent purely fluvial channel filling with bottom reworking lag deposits (Facies Gt and Gh from Miall, 1996). However the presence of ichnofabric *Arenicolites* (and possible *Dactiloides*?) observed at the top of this facies (Fig. 6-C) and the presence of the benthic foraminifer *Karreriella conversa* (Facies A4) suggest deposition in, respectively, tide-influenced environment (deltaic or estuarine) and deposition in shallow marine platform with continental influx (see Table 1). Facies association A is therefore related to both tidal and fluvial environments.

Reactivation surfaces as observed within the cross-bedded sandstones of Facies A1 can be caused by tidal current reversals (Klein, 1970; de Mowbray and Visser, 1984) even if these surfaces could also be produced by river-discharge variations and erosion of brink by arrival of a new

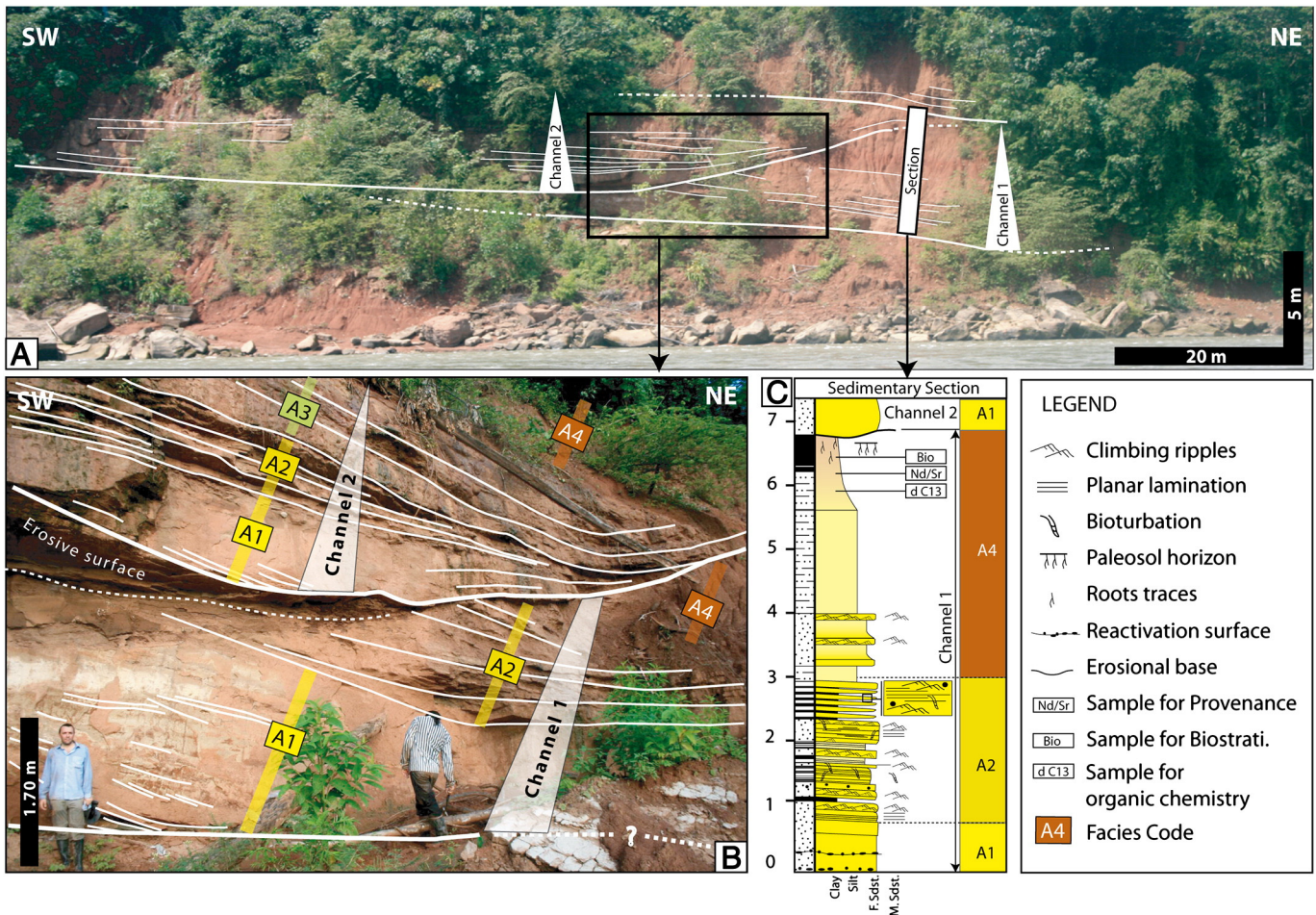


Fig. 5. Outcrop MD-255. A) General outcrop view along the river cutbank. B) Zoom from A. Interpreted photograph of two stacked channels. C) Sedimentary section with Facies code (see Table 2 for details).

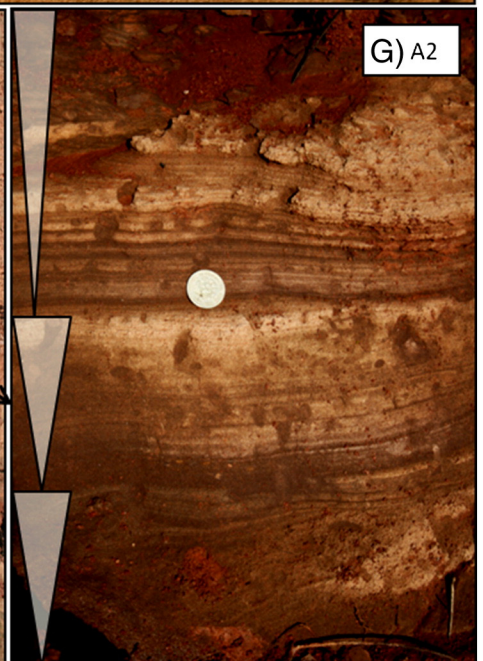
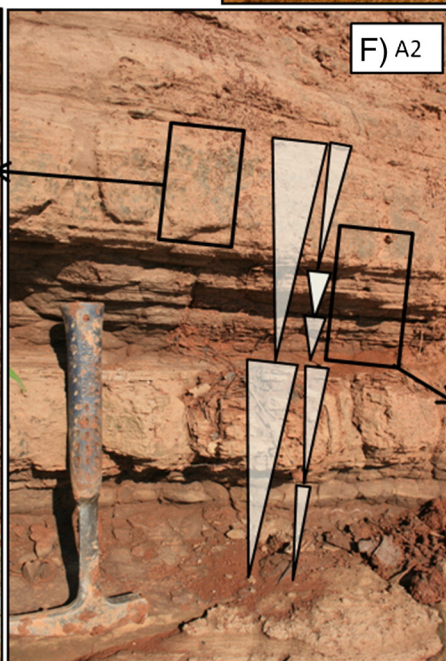
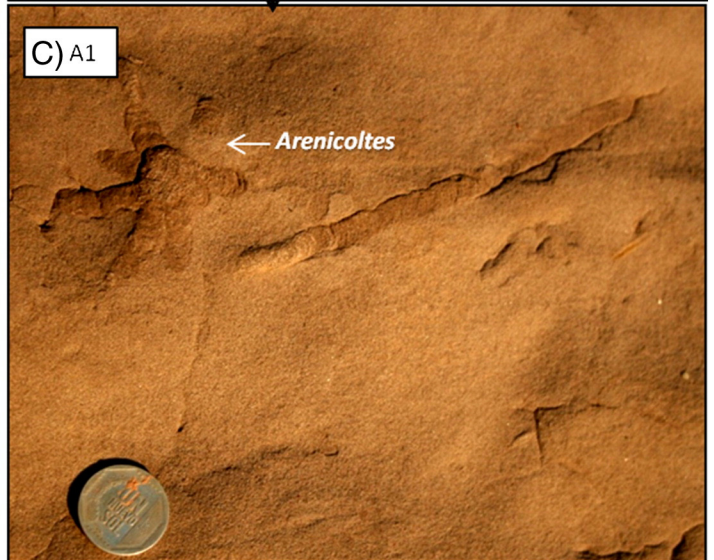
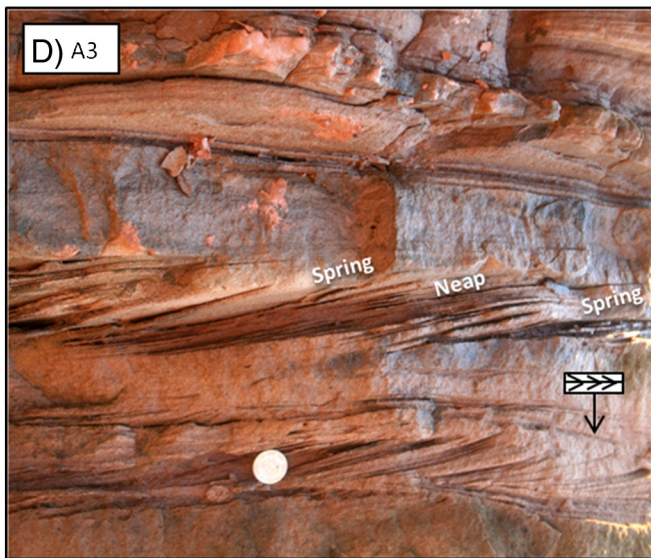
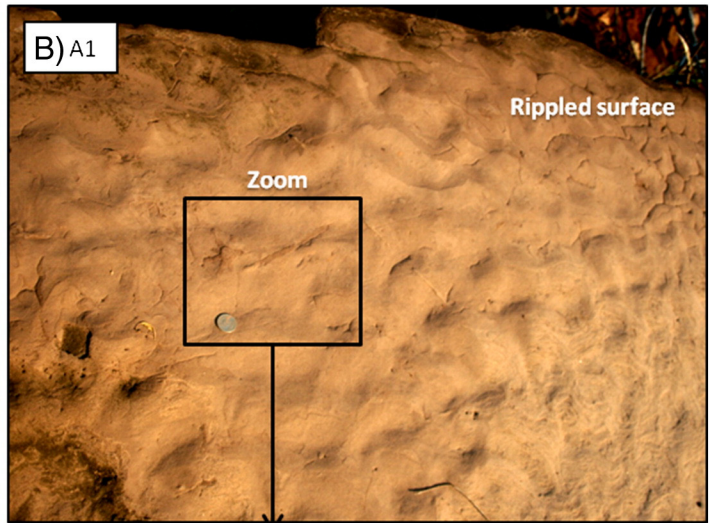
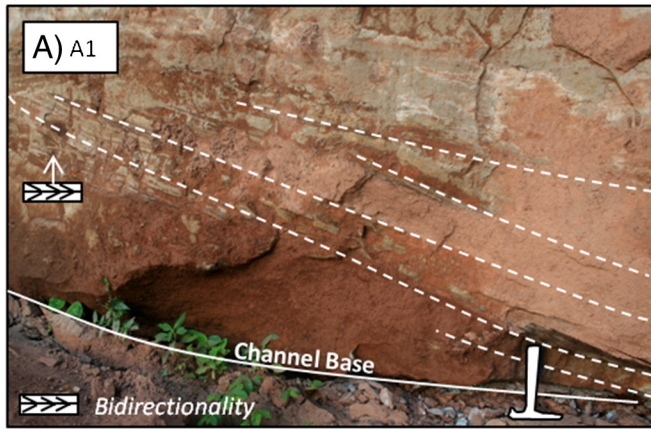
bedform in fluvial settings (Dalrymple, 1984). The occurrence of rare bidirectional trough cross-bedding (Fig. 6-A) suggests a depositional area receiving opposite-direction currents, dominated either by flood or ebb currents. The prograding pattern displayed by the tangential cross-bedded sandstones suggests lateral accretion processes. Mud clasts have been deposited at the base of the channels by gravity processes. They are common in channel bottom deposits in many tide-dominated or influenced environments because of the erosion by high-energy currents of thin muddy layers forming slack water drapes, or because of the erosion by lateral accretion of muddy tidal-flat and salt-marsh deposits (Dalrymple and Choi, 2007). In conclusion, we interpret Facies A1 as dune deposits formed during the early-stage of a tide-influenced channel settlement controlled by both fluvial and tidal processes.

Facies A2 and A3 overly the basal filling of the channelized bodies and constitute small-scale Inclined Heterolithic Stratification (IHS). These IHS developed by lateral accretion within the channels (Fig. 5-A and B). Although IHS may be observed in fluvial environments (e.g., Jackson, 1981; Page et al., 2003), they are most common in tide-influenced settings (Dalrymple et al., 2003). In addition, Facies A2 and A3 often display rhythmic patterns and heterolithic textures. Interlamination of mud and fine-grained sands results from suspension and weak traction current and may occur in fluvial overbank deposits (lithofacies Fl, Miall, 1996). However, alternation of sand and mud laminae within millimetric wavy and flaser beddings (Facies A2 and A3) is more frequent in tidal depositional environment. Concerning Facies A2 and A3, the abundance of wavy and flaser bedding, mud drapes and rhythmicity rather suggests tidal influence on deposition (Nio and Yang, 1991). Recurrent thickness fluctuations observed within the cross-bedded sandstones in the

successive sandy beds of Facies A3 (Fig. 6-D) may be interpreted as the result of neap-spring influence (Eriksson et al., 1998; Eriksson and Simpson, 2004; Mazumder and Arima, 2005). Similar rhythmicity has also been found within facies A2 (Fig. 6-F and G). The presence of few thin mud drapes observed within these sandstones may therefore represent deposition during tidal slack-water periods. Facies A2 corresponds to lower hydrodynamic conditions than Facies A3 (coarser sandstones). However, they both constitute IHS, and are interpreted to have been deposited by lateral accretion in a channelized body. Therefore, Facies A2 and A3 are both interpreted as tide-influenced point-bar deposits in a meandering channel. Because Facies A3 is situated above Facies A2 (Fig. 5), Facies A3 should be related to a higher energy recovery during the channel deposition history.

Facies A4 corresponds to the uppermost- and finest strata deposited at the top of the channel succession. This silty facies could firstly be interpreted as channel abandonment, fluvial floodplain or tidal-flat deposits. The presence of *Karreriella conversa* indicates deposition in a coastal, brackish water environment (Valchev, 2007) and supports a tidal flat interpretation for Facies A4. According to Dalrymple and Choi (2007), the pedogenic structures described in the mudstones at the top of Facies A4 could be associated to a period of emersion of a tidal mud flat.

To conclude, Facies association A corresponds to a moderate-energy channel filling history. According to the IHS geometry resulting from lateral accretion processes, this channel is interpreted to be related to a meandering system. Because of the proximity of pedogenetic features and because of the preponderance of fine-grained texture in the facies association, this meandering system could be purely fluvial.



However, the evidences of tidal- or marine-related environment (benthic foraminifer, *Arenicolites*) and the evidences of tidal-processes (rhythmic patterns, IHS, mud drapes) finally suggest a mixed fluvial–tidal environment. Facies association A is interpreted to correspond to the sedimentary infilling and abandonment of tide-influenced meandering channels migrating laterally in surrounding tidal-flats and floodplain.

4.2.2. Facies association B: tide-dominated environment

4.2.2.1. Description. Facies association B consists of 5 facies: B1, B2, B3, B4 and B5. They all have been found in MD-256 (Fig. 7) and partially in MD-85 (Fig. 9) and are summarized in Table 2.

Facies B1 corresponds to the infill of isolated channelized sedimentary bodies (~60 to 150 m width and ~1 to 1.50 m in thickness) and has been observed at both MD-256 and MD-85 localities. No stacking or amalgamated pattern has been noticed. The base of this facies corresponds to a channel-shaped surface. This surface is highlighted by elongated millimetric to centimetric mud clasts forming a breccia of few centimeters-thick and evolving upwards into massive medium- to fine- or very fine-grained sandstone. Internal sigmoid cross-beddings (45 cm in height) are often present in the basal part of these sandstones. Fine-grained sandstones may also display high-angle climbing ripples at their base evolving upwards into low-angle climbing ripples (Fig. 8-A). At the top of the deposits, climbing ripple cross-stratification changes upward into more flattened trough cross-stratification (see channel sedimentary structures within the channel of outcrop MD-85, Fig. 8). Reworked charophyte oogonia, stingray teeth (MD-85), and benthic foraminifer (MD-256) are observed in this facies (Table 1).

Facies B2 (total thickness of ~20 m) consists of reddish mudstones. Root traces and gypsum or anhydrite nodules can develop at the top of the facies (Fig. 8-B). This facies has been observed at the top of the sedimentary section and presents a sharp contact with the underlying facies B3 (Fig. 7). It is also laterally associated with Facies B1.

Facies B3 and B4 are closely related and often alternate in the section described (Fig. 7). In this case, the contact between the two facies is sharp. Facies B3 (total thickness of 0.50 to 4 m) consists of bioturbated and burrowed reddish mudstones to rare siltstones. Occasional lenticular bedding can occur within the mudstones. Facies B4 (total thickness of 1 to 5 m) corresponds to highly burrowed heterolithic deposits showing regular alternations of very fine to fine-grained sandstones with muddy or silty layers displaying planar horizontal, wavy bedding and lenticular bedding (sets of 10 cm thick) (Fig. 8-C, D and E). Burrows are horizontal or vertical but no specific ichnofabric can be determined (Figs. 8–4D). Color is dark gray to violet. The sedimentary structures in sandstones are highlighted by thin (2 to 3 mm thick) laminae of mud and silty drapes. Thin sand layers can occasionally be intercalated by mud drapes, thus forming mud couplets. Opposite current dips have been observed in this facies. At the top of sandy strata, fluid escape structures can be observed (Fig. 8-E). Facies B5 (total thickness of ~20 cm) is generally observed above Facies B4, after a sharp or progressive contact (Fig. 7). It is made up of clean fine-grained sandstone often ending with a wave-rippled surface (ripples are 1 to 1.5 cm in height with wavelength of 6.5 to 8.5 cm) (Fig. 8-F).

4.2.2.2. Interpretation. Facies B1 corresponds to channel infill deposits. Climbing-ripple cross-stratification is a common feature in a wide range of depositional environments in which suspension exceeds the rate of traction transport (Jopling and Walker, 1968; Allen, 1970; Ashley et al., 1982). However, sigmoidal cross-bedding associated with the presence of brackish-water fossils (benthic foraminifer, see Table 1) suggests deposition within a tide-influenced environment.

Climbing ripples from tidal environments are different from non-tidal climbing ripples by having common mud drapes and finer-grained texture (Choi, 2010). In a tidal environment, they can be characteristic of tidal inlet infillings in the fluvial–tidal transition zone of estuaries (Dalrymple et al., 1992; Tessier, 1996; Hovikoski et al., 2008). Flood dominated Climbing Ripple Facies (CRF) can also be associated with tidal channel levees found in the inner/straight channel zone of the fluvial–estuarine transition (cf. Mont St Michel estuary; Tessier, 1996). In case of ebb-dominated context, CRF are found in chute channels and chute bars in the meandering zone of the fluvial–estuarine transition (Tessier, 1996). In comparison with Facies A1, Facies B1 is finer-grained and is related to decreasing flow processes (climbing ripples). Geometrically, Facies B1 only concerns isolated channels whereas Facies A1 is related to stacked and thick channels overlain by laterally migrating strata (IHS deposits; Facies A2 and A3, Fig. 5). Channels from Association A represent higher energy channels in comparison with those from Facies association B (Facies B1). We interpret Facies B1 as tidal inlet deposits. Facies B2 is generally structureless but contains paleosol horizons and gypsum nodules in a very fine shaly matrix. As it is laterally associated with Facies B1, it has been interpreted as saltmarshes in a supratidal environment. Facies B3, characterized by muddy deposits with scarce lenticular bedding, could correspond to mud flat deposits in an intertidal environment. Facies B4 is characterized by highly burrowed heterolithic deposits with double mud drapes, wavy and lenticular beddings that are typical sedimentary structures of tide-influenced environments (Nio and Yang, 1991; Dalrymple et al., 1992; Dalrymple and Choi, 2007). We consequently interpret Facies B4 as mixed muddy/sandy flat deposits.

To conclude, Facies association B is constituted by all the surrounding flats influenced by tidal processes, from the subtidal area (tidal inlet (Facies B1), mixed tidal flats with double mud drapes (Facies B4 and B5) to the intertidal/supratidal environments (mud flats and saltmarshes, respectively Facies B2 and B3).

4.2.3. Facies association C: bay and shallow marine environments

4.2.3.1. Description. Facies association C is composed of six facies: C1, C2, C3, C4, C5 and C6. All the facies have sheet-like geometries, and have been described at outcrops MD-85 (Fig. 9), MD-177 and MD-184 (Fig. 10, Section 1 and 2, respectively).

Facies C1 (total thickness of 50 cm to >2 m) corresponds to blue–violet–reddish marls to carbonated siltstones with centimetric thick fine-grained sandy layers and occasional centimetric thick carbonaceous layers (Fig. 11-A). Ripples and climbing ripples are present within the sandy layers. Facies C1 contains benthic foraminifer (*Bathysiphon*, Fig. 11-B), Mollusca (Bivalvia: *Corbicula* and *Polymesoda*; Gastropoda: Cerithioidea, Pachychilidae, and ?*Aylacostoma*), Ostracoda, Chondrichthyes (Myliobatiformes: *Ouledia* sp., Pristidae, and Dasyatoidea), and Osteichthyes (Pycnodontiformes: *Coelodus*; Characiformes: Serrasalminae and indet.) (see Table 1). Facies C2 (total of thickness 80 cm to 1 m) is always closely related to Facies C1 and the contact (basal and top) between the two facies is progressive. Facies C2 is similar to Facies C1 but contains common sandy and gypsum nodules, root traces and bioturbation. Facies C3 (total thickness of 15 to 50 cm) corresponds to millimetric to centimetric sandy nodules scattered into a violet muddy to silty matrix, forming a matrix-supported breccias. This facies contains numerous organic fragments such as fish vertebrae and ostracods. Facies C4 corresponds to an alternation of marl (5 to 10 cm) and thin limestone strata (2 to 5 cm). Carbonate nodules are frequent within the marls. Limestones commonly present well-developed desiccation crack surfaces at the top of the strata as

Fig. 6. Facies photographs for Facies association A (FA-A). A) Facies A1, showing fine-grained sandstone with tangential cross-bedding and sets prograding in the same direction. Note that bidirectionality has been observed in this facies. B) Photograph of the rippled-surface of Facies A1. Square indicates the location of photograph C. C) Ichnofabrics from Facies A1 top surface: *Arenicolites* and possible *Dactiloides* (tubular trace). D) Facies A3. Tangential cross-bedding with planar laminations at their base. Rare asymmetrical ripples in the opposite direction can also be observed at the top of the tangential laminations, suggesting bidirectionality. Regular changes in thickness suggest cyclicity, possibly Neap and Spring cycles. E) Photograph of climbing-rippled cross-stratification of Facies A2, from the zoom section displayed on F. F) View of the heterolithic and cyclic deposits of Facies A2. Black squares indicate the location of photographs E) and G). G) Photograph of Facies A2, with massive fine-grained sandstones or flaser bedding alternating with wavy- or planar muddy lamination.

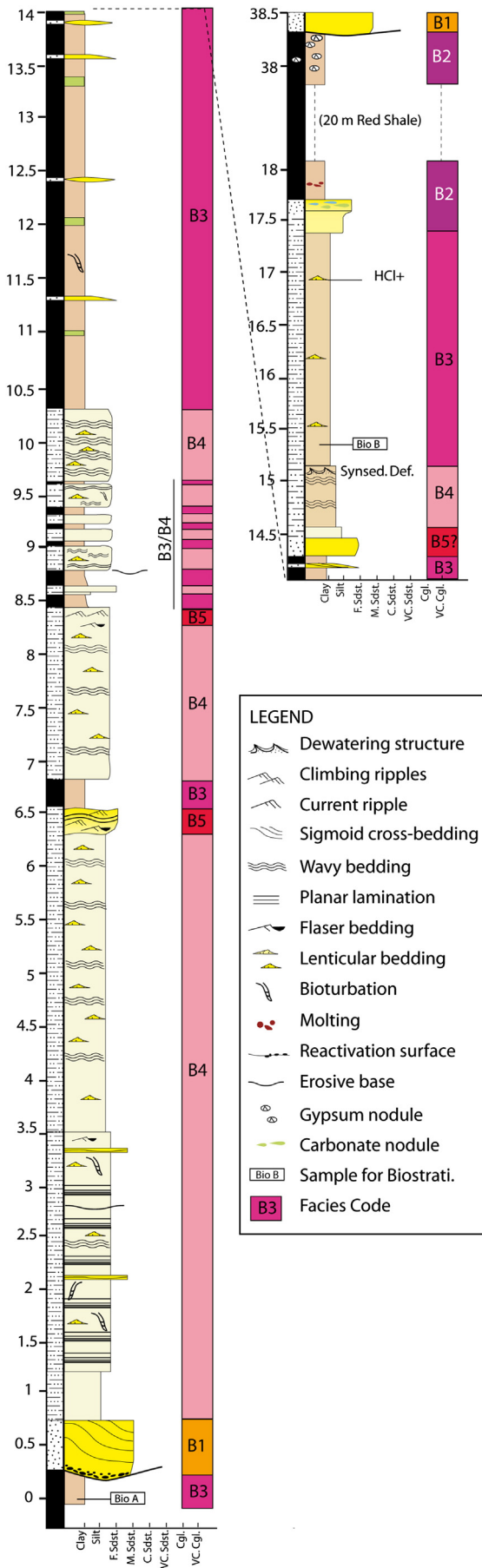


Fig. 7. Sedimentary section from outcrop MD-256.

well as burrows and root traces. Small oyster shells (2 to 4 cm in length) are visible within the limestone strata. Microfacies analysis of thin sections allowed the recognition of oysters (little size species), fish vertebrae fragments, annelid burrows, numerous ostracods and/or phylopods, and undifferentiated gastropods (Fig. 12-A, B, C and D). Only very few ostracods and phylopods present a complete carapace with paired valves but they all present a smooth surface. According to Dunham's classification (Dunham, 1962), the observed limestones can be classified as wackstone to packstone. The matrix is generally micritic or microsparitic. Peloidal micrite (Fig. 12-A and B) could constitute secondary cementation better than primary matrix. Secondary sparite grains are common, and can form druse or bird-eye cements (Fig. 12-B and D). Facies C5 (strata presenting thickness of 25 to 80 cm) also corresponds to limestone deposits showing desiccation cracks at the top (Fig. 11-C and D). These strata present undulated base and top. Thin-section shows stromatolith filaments entangled with ostracod carapaces and annelid burrows (Fig. 12-E and F). The matrix is micritic to microsparitic. Facies C6 corresponds to limestone strata (10 to 25 cm thick) with abundant small-size oysters (2 to 4 cm in length). Thin-section reveals numerous oysters with lamellar and multilayered structures, annelid burrows, blue (?) algae filaments, fish coprolith and some ostracodes (Fig. 12-G, H, I and J). Root traces are also present. The matrix is made up of micrite or small microsparite crystals. Some bivalve's shells are rounded by a micrite envelope (Fig. 12-G). This facies is separated from the other because of its greatest oyster content.

4.2.3.2. Interpretation. The ichthyofauna from Facies C1 and C3 is characteristic of a shallow marine environment, with variations from a strong freshwater influence in a more proximal environment to a confined and steady proximal marine environment of normal salinity (as attested by the wide array of obligate marine taxa, such as chondrichthyans and pycnodontiform actinopterygians; Cappetta, 2012). Absence of high energy sedimentary structure in Facies C1 suggests deposition in a protected shallow marine environment. Pedogenic structures of Facies C2 are related to episodic emersions of these shallow-marine deposits (originally Facies C1). Facies C3 is interpreted to have been deposited by an episode of higher energy in this shallow marine environment, maybe related to bank collapsing. Facies C4, C5 and C6 correspond to limestones deposited in a subaquatic environment submitted to frequent subaerial exposures as attested by the desiccation cracks and root traces and burrows found at the top of the beds. The presence of little-sized oysters (characteristic of a stressed environment), smooth-carapace ostracodes and annelids is consistent with a shallow marine environment (Armstrong and Brasier, 2005) whereas micrite envelopes rounding bivalve's bioclasts indicate an intertidal context. Evidences of frequent subaerial exposures indicate a short-lived and frequently changing depositional environment, from intertidal to lacustrine. Stromatolithic carbonates of Facies C5 are related to a confined and stressed intertidal environment (Wattinne, 2004), whereas the *Ostrea* limestones of Facies C6 are in agreement with a deeper confined marine environment (Enay, 1990) intertidal to upper infralittoral. Because of the presence of some fresh water fossils and the occurrence of frequent emersion, the depositional setting should be quite close to the coast. To conclude, we interpret Facies association C to represent deposition in a bay/lagoon or stressed shallow marine-environment.

4.3. Organic geochemistry

The TOC contents of the samples were in general very low, ranging from 0.03 to 0.06 wt.% (Table 3). Therefore, care should be taken to interpret the organic geochemical data. Nonetheless, the reproducibility of TOC contents and $\delta^{13}C_{TOC}$ was better than 0.02 wt.% and 0.3‰, respectively. The $\delta^{13}C_{TOC}$ values varied from -23.4 to -29.8‰ (Table 3).

The $\delta^{13}C_{TOC}$ of higher plants that use the Calvin-Benson cycle of carbon fixation (i.e. so-called C₃ plants) ranges from -29.3 to -25.5‰,

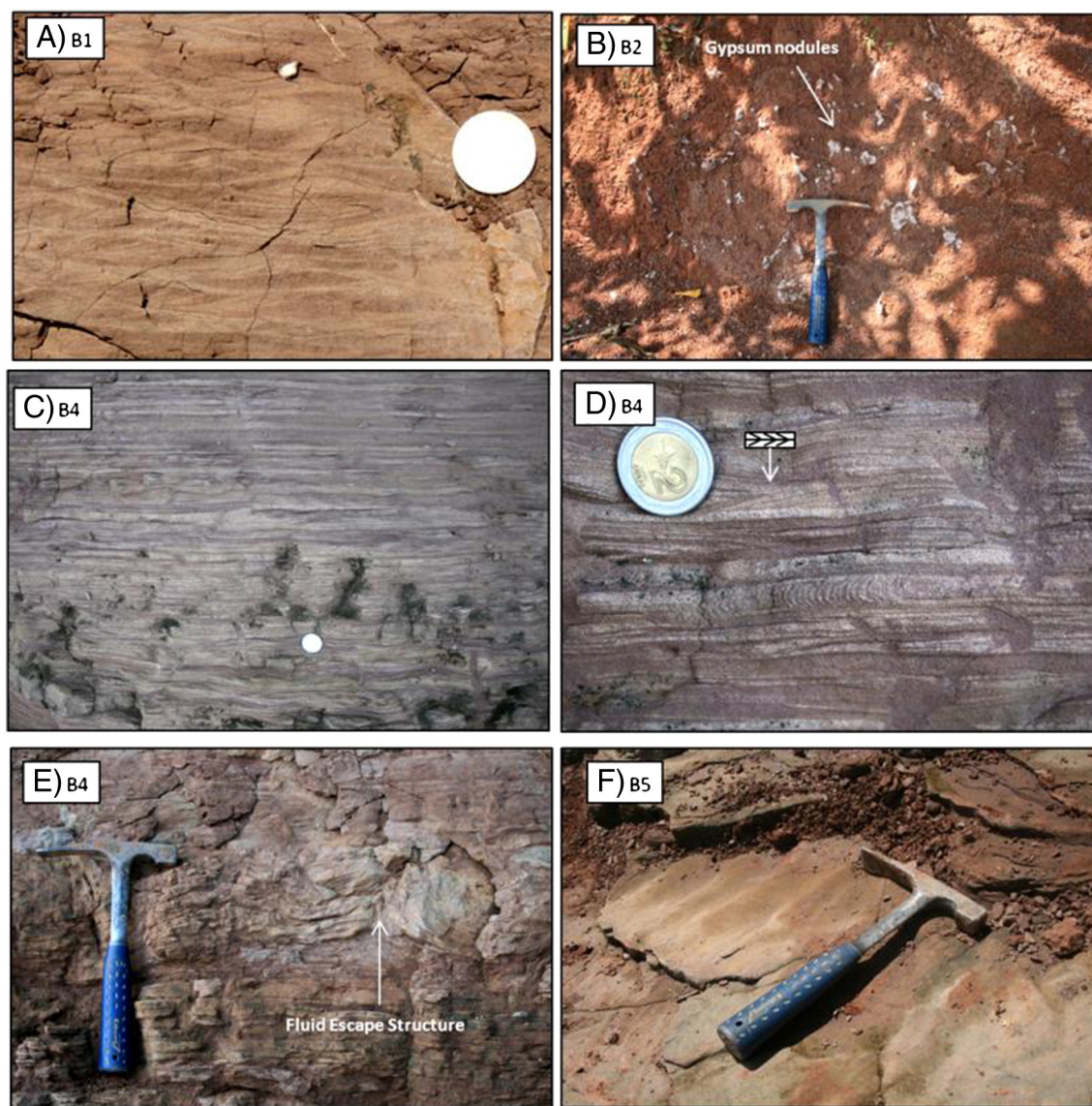


Fig. 8. Facies photographs of Facies association B (FA-B). A) Fine-grained sandstone with climbing ripples. B) Root traces and gypsum or anhydrite nodules developing at the top of the reddish mudstones of Facies B2. C) Facies B4. Highly burrowed heterolithic deposits showing regular alternations of very fine to fine-grained sandstones with muddy or silty layers displaying planar horizontal and wavy bedding. D) Horizontal and vertical burrows in Facies B4. E) Fluid-escape structure within deposits of Facies B4. F) Facies B5 with rippled-surface.

with an average value of about -27% (e.g. Tyson, 1995). The typical marine $\delta^{13}\text{C}_{\text{TOC}}$ values are in the range of -18 to -22% (e.g. Meyers, 1997). The $\delta^{13}\text{C}_{\text{TOC}}$ values (-27.3 to -29.8%) of MD-177, MD-85, and MD-255 are hence typical of C_3 plant-derived organic matter. In contrast, the $\delta^{13}\text{C}_{\text{TOC}}$ value (-23.4%) of MD-184 is enriched in ^{13}C compared to the other samples, closer to typical marine $\delta^{13}\text{C}_{\text{TOC}}$ values. This suggests the presence of substantial amounts of aquatic organic matter in MD-184. Notably, it has been shown that the presence of a freshwater algae *Pediastrum*, which is very common in lagoonal settings, can cause substantially enriched $\delta^{13}\text{C}_{\text{TOC}}$ values, up to 2% (e.g. Steurbaut et al., 2003). Consequently, our organic geochemical results suggest that organic matter in MD-184 might be dominantly derived from aquatic (marine or lagoonal) environments. This interpretation is supported by additional rock-eval analysis results obtained for MD-184, indicating Type II kerogen, which originates from mixtures of zooplankton, phytoplankton, and bacterial debris in marine sediments (Peters and Cassa, 1994). The three other samples (from outcrops MD-85, MD-255, and MD-177) indicate a possible mixed organic matter

origin, from terrestrial to brackish environments, but are more characteristic of terrestrial environment.

4.4. Nd–Sr isotopic composition

The Nd–Sr isotopic compositions of the Thanetian sedimentary rocks are shown in Table 4. Overall, the sediments have quite variable $\epsilon\text{Nd}(0)$ values (ranging from -6.2 to -10.7) with a comparatively narrow range of $^{87}\text{Sr}/^{86}\text{Sr}$ compositions (0.712024 to 0.719026) (Table 4). The four samples analyzed for their Nd–Sr isotopic compositions have been reported in the $^{87}\text{Sr}/^{86}\text{Sr}$ versus $\epsilon\text{Nd}(0)$ diagram (Fig. 13). The isotopic results are compared with several other relevant source fields: Mesozoic and Neogene volcanic rocks (Rogers and Hawkesworth, 1989; Kay et al., 1994); Quaternary Ecuadorian lavas (Barragan et al., 1998); Cenozoic sedimentary rocks from the Depression, Altiplano, Oriental Cordillera and Subandean zone of Chili and Bolivia (Pinto, 2003); modern suspended sediments from the Solimoes and Madeira rivers (Viers et al., 2008); Neogene deposits from the Amazonian foreland basin of Bolivia,

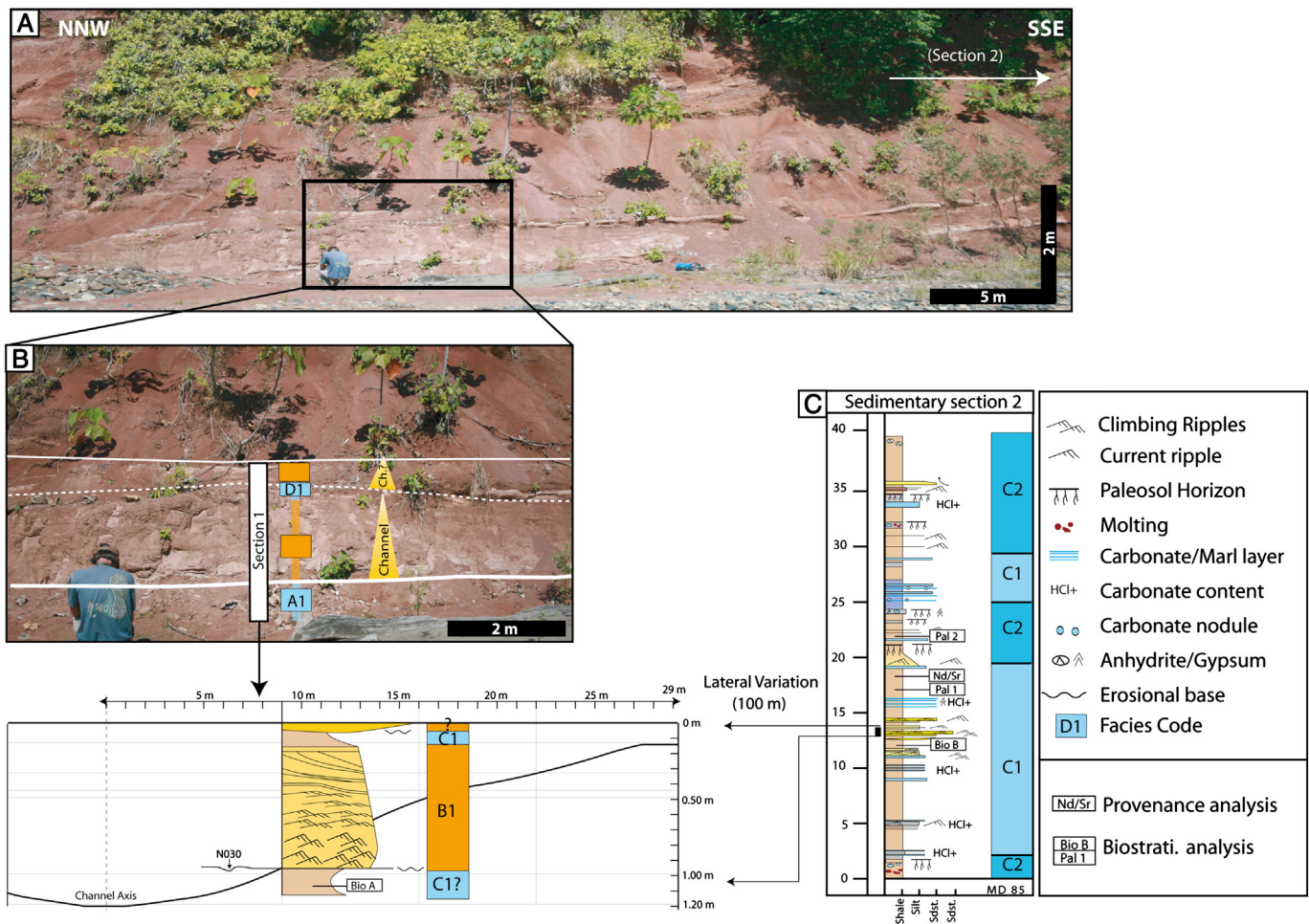


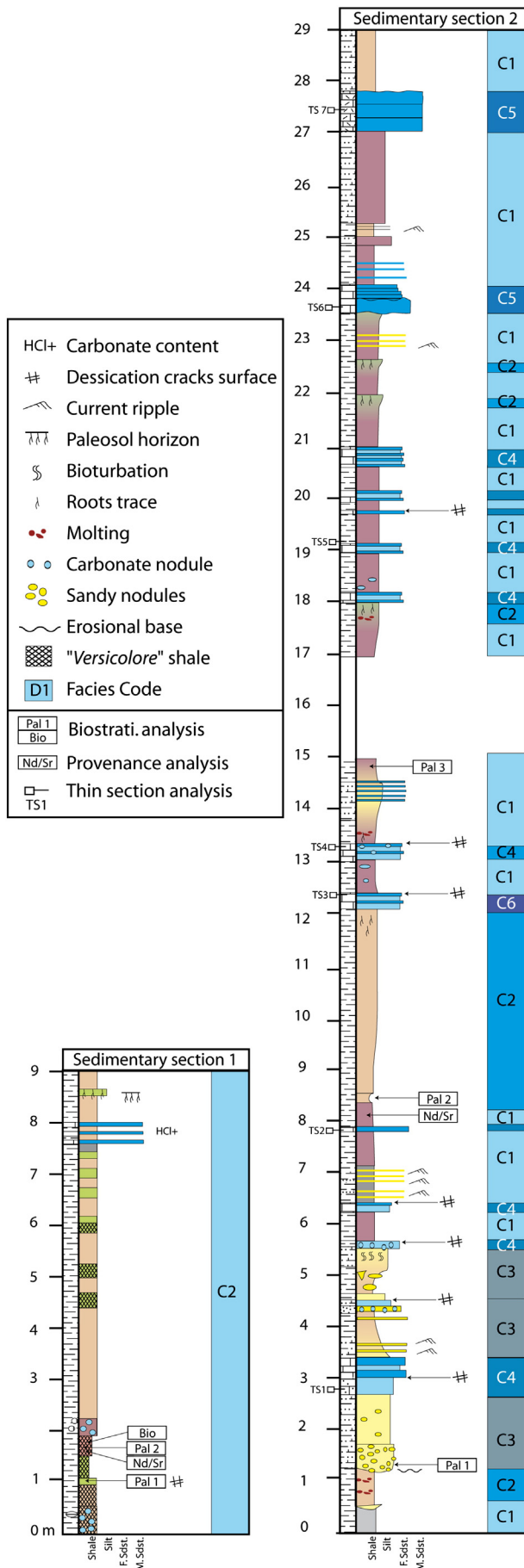
Fig. 9. Outcrop MD-85 near Pantiacolla anticline. A) General view of the outcrop. Black rectangle precise the location of photograph B. B) Enlarged view from A with the location of the sedimentary Section 1 described. C) Sedimentary Section 2 and Facies code. Note that 100 m separates the two sedimentary sections.

Ecuador and Peru (Roddaz et al., 2005a), and the sand of the Peruvian White Sand (WS) Formation cratonic in origin (Roddaz et al., 2005a). Nd–Sr isotopic compositions of sediments deposited by an Andean drainage define plot within a mélange hyperbole as observed by Basu et al. (1990), Roddaz et al. (2005a) and Roddaz et al. (2012) for Neogene sediments of the Amazonian foreland basins, with one end member being the primitive volcanic arc and the other the upper continental crust of the Brazilian shield. The four analyzed Paleocene samples plot within the field of the Cenozoic Altiplano sediments, indicating a similar Andean provenance. When compared with Neogene Subandean zone sediments, they plot closer to the volcanic arc end member, indicating a greater contribution of the volcanic arc rocks end member for the Paleocene sedimentary rocks relative to Neogene SAZ sediments.

5. Depositional environment synthesis

Our biostratigraphical results, sedimentary facies interpretations and organic geochemistry analysis indicate the presence of a tide-influenced shallow marine paleoenvironment during the Paleocene in the northern Madre de Dios basin. Facies association A corresponds to the sedimentary filling of a tide-influenced meandering channel deposited in the fluvial-tidal transition zone. Facies association B corresponds to tidal flats deposits, tidal inlets and also characterizes a tide-influenced environment but with more distal facies than Facies association A. Facies association C, interpreted as deposited in a bay/lagoon or stressed shallow marine environment, is the most distal facies association. The facies of this association do not show any evidence of tidal nor oscillatory currents.

The transition between the land and the sea in tide-dominated coastal environments is among the most complex on Earth, because of the interaction of numerous physical, chemical and biological processes (Dalrymple and Choi, 2007). Existing depositional models are therefore preliminary because the number of case studies of many of the subenvironments is rather small (Dalrymple and Choi, 2007). However, our dataset makes the possibility to distinguish between tide-dominated delta and tide-dominated estuary. First, from a geological point of view, estuaries are transgressive whereas deltas are regressive (Dalrymple et al., 1992). The tide-dominated Paleocene deposits studied in this paper overly continental deposits of the Yahuarango Formation. This stratigraphic succession therefore suggests that the tide-dominated Paleocene deposits are transgressive and related to an estuary. The presence of a Paleocene tide-dominated estuary is further attested by the occurrence of a well expressed tide-influenced meandering zone. According to several works (Dalrymple et al., 1992; Dalrymple and Choi, 2007), only the fluvio-estuarine transition zone in a tide-dominated estuary could explain the occurrence of both opposite currents and meandering channels in a tide-influenced environment. Facies association A could be an illustration of this fluvial-tidal environment, as it shows evidences of meandering channels influenced by both fluvial and tidal currents (Fig. 14). According to this interpretation, Facies association B could be interpreted as deposited in the outer part of this tide-dominated estuary, where tidal inlets are still present and can laterally be connected to muddy and mixed tidal-flat deposits (Fig. 14). Finally, as Facies association C does not show any evidences of tidal currents, we suggest deposition in a shallow confined marine environment (Fig. 14).



6. Paleogeographic and tectonic implications

The data presented in this study document for the first time the existence of Paleocene tide-dominated estuary debouching into a shallow marine bay in the western Amazonian foreland basin. We favor a Thanetian age for this marine incursion but a Danian age cannot be discarded. Most of Paleocene sedimentary rocks of other parts of the Andean/Amazonian foreland basin were mainly deposited in a distal fluvial environment (see Fig. 2 and references therein). The presence of estuarine deposits overlying continental deposits indicates a marine transgression during the Paleocene. This transgression is caused by an increase in accommodation space which in turn depends on the interplay between sediment supply and base level changes (see Catuneanu, 2004 and references therein). In a retroarc foreland basin setting, numerous mechanisms can be envisaged to account for an increase in accommodation space including eustasy, mantle processes, foreland related tectonics (i.e. loading/unloading cycles of Catuneanu et al., 1997) and decrease in sediment supply. The Danian and Thanetian periods are characterized by a drop in global sea-level (Fig. 3) (Haq et al., 1987; Hardenbol et al., 1998; Vandenberghe et al., 2012). Consequently the recorded transgression (Danian or Thanetian in age) is not related at first order to a rise in global sea-level. Dynamic loading may be induced by subduction beneath the retroarc foreland basin. Subduction generates long wavelength subsidence (Mitrovica et al., 1989; Catuneanu et al., 1997; Pysklywec and Mitrovica, 2000; Catuneanu, 2004) capable of maintaining the four depozones of the foreland basin system below the base level (Catuneanu et al., 1997; Catuneanu, 2004) and thus of producing accommodation at the basin scale. In fact, we have no idea of the depositional environment of other depozones (wedgetop, proximal foredeep and backbulge) adjacent to our study area so that it is difficult to exclude subsidence dynamic as a possible mechanism. However, the presence of a Paleocene flexural forebulge in the southern Bolivia foreland basin caused by loading of the Western Cordillera (DeCelles and Horton, 2003) suggests that Andean tectonic loading was a first-order control on tectonic subsidence in Paleocene times. This is in agreement with our Nd–Sr isotopic provenance data that show an Andean provenance and hence the presence of an Andean relief in Paleocene times. Short-lived marine incursions controlled by tectonic loading have also been documented in the Upper Cretaceous Western Canada foreland system (Catuneanu et al., 1999). Shallow marine incursions provoked by Andean tectonic loading have already been documented in the Amazonian foreland basin system (Roddaz et al., 2010) and in the Bolivian retro-arc foreland system (Hernandez et al., 2005). Based on the relatively little thickness of the marine deposits documented in the Madre de Dios basin (40 to 50 m thick outcropping section), we propose that Paleocene marine strata probably correspond to a single high-frequency cycle as defined by Catuneanu (2004). Based on the fact that these higher-frequency cycles are mainly controlled by tectonism in the adjacent belt (Catuneanu, 2004), and based on the relatively low sea-level stage during Paleocene period, we suggest that the marine incursion documented in southern Peru was mainly caused by Andean tectonic loading although additional mantle driven subsidence cannot be excluded.

The entrance of this Paleocene marine incursion (Atlantic Ocean, Pacific Ocean or Caribbean Sea) remains to be elucidated. Very few Paleocene marine or coastal deposits are documented in the Andean/Amazonian foreland basins. Paleocene formations of Ecuador and elsewhere in Peru show no evidences of marine or coastal deposits (Fig. 2). In the Bolivian Altiplano and the Eastern Cordillera there is no evidence of any marine influence attested so far except during Danian times in Potosi, Bolivia (El Molino Formation; e.g. Cappetta and Gayet, 2013). Hence the Paleocene paleogeographical map proposed

Fig. 10. Sedimentary sections from outcrop MD-177 (Sedimentary Section 1) and MD-184 (Sedimentary Section 2).

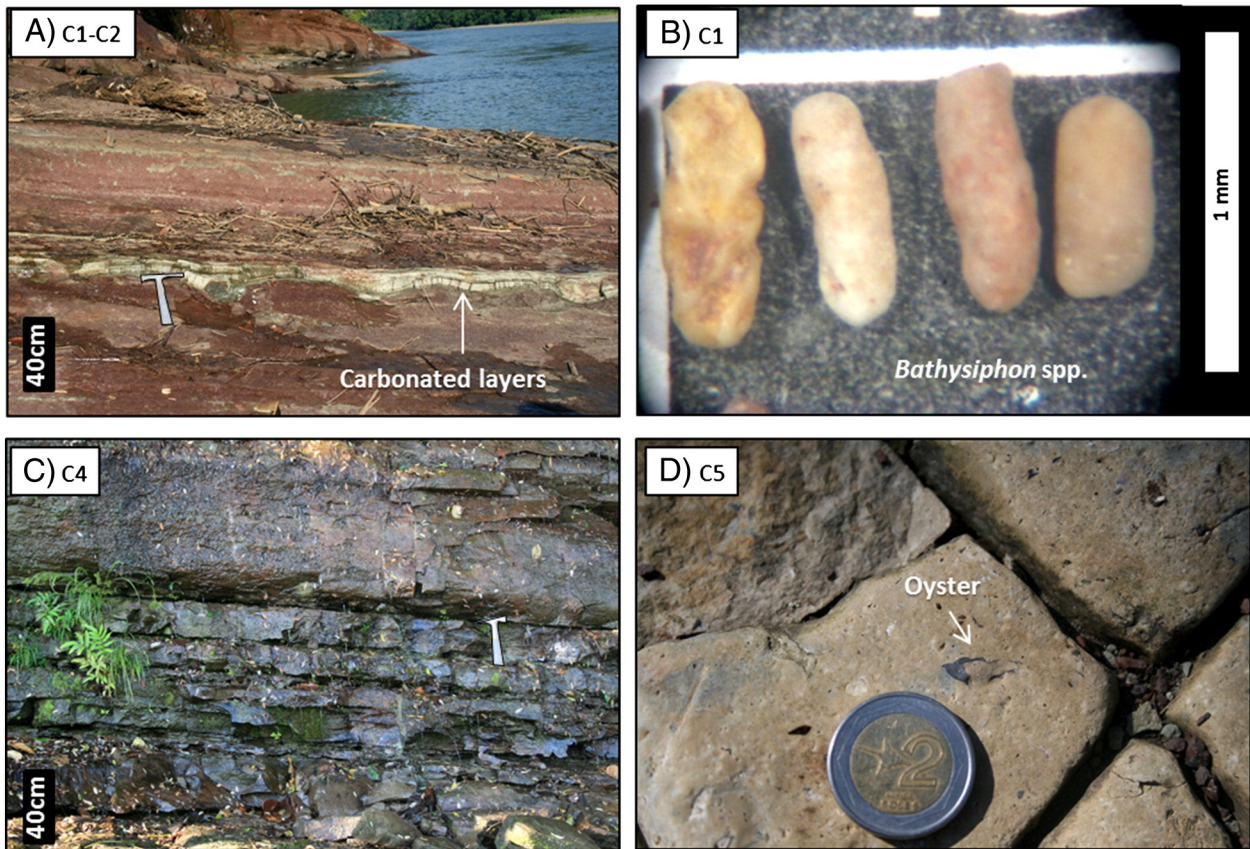


Fig. 11. Photographs from outcrop MD-184. A) Outcrop view of alternating Facies C1 and C2. Note undulating marls/carbonated layers. B) Benthic foraminifer *Bathysiphon* sp. found in Facies C1. C) Outcrop view of carbonated layers from Facies C4. D) Desiccation cracks at the top of a carbonated layer in Facies C5. Note little-sized oyster visible on that surface.

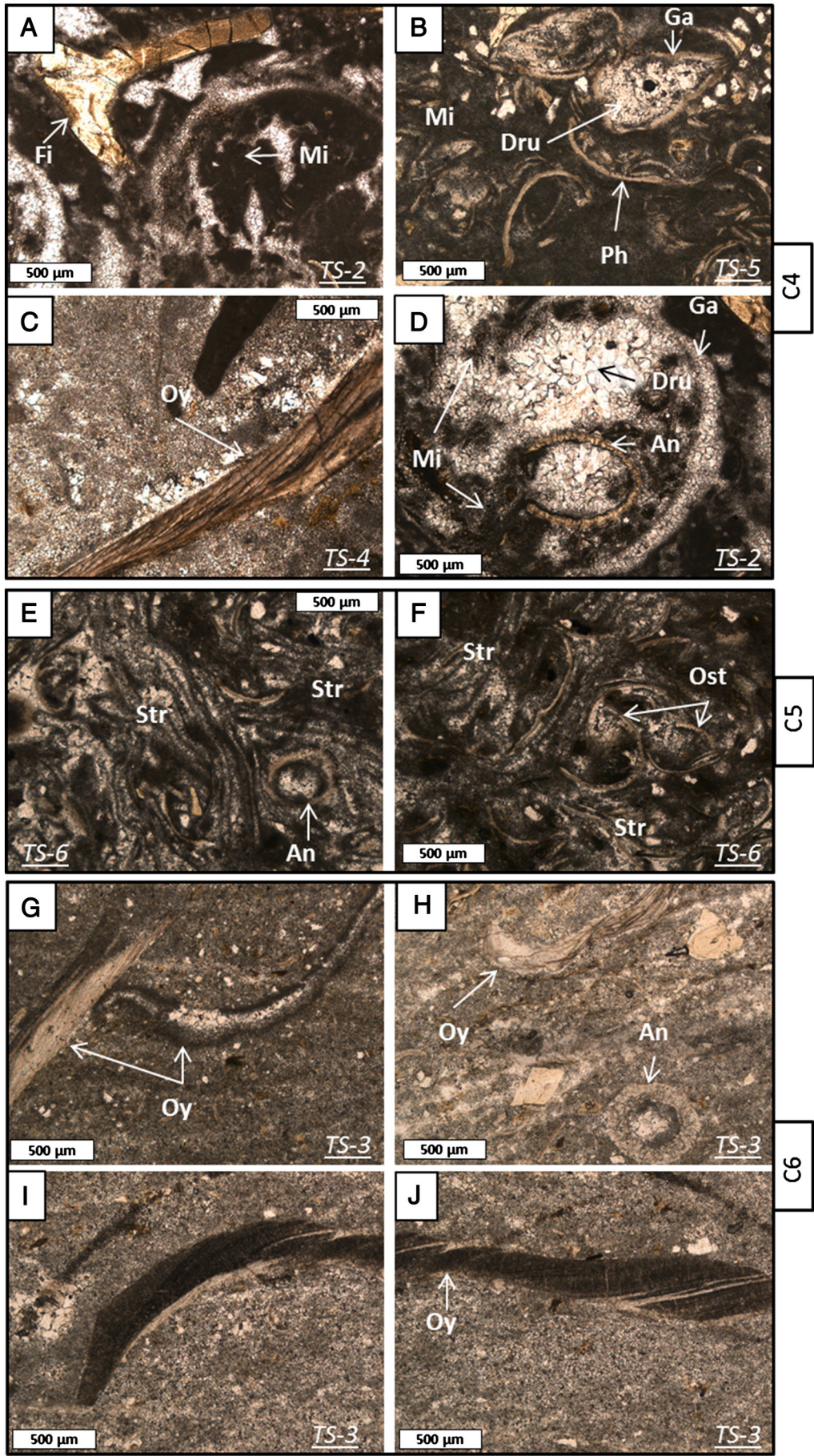
here is tentative (Fig. 15-A). In conjunction with the absence of shallow marine deposits in North-western South America, our data might suggest a southern connection with the Atlantic Ocean (Bolivia–Argentina). In any case, more detailed sedimentological works are needed to decipher the locus of this Paleocene marine entrance. The Paleocene marine transgression documented here predates a well-known Eocene transgression occurring in the Colombian, Ecuadorian and northern Peruvian Amazonian foreland basins and recorded by the Lower Carbonera, Orteguzza and Pozo Formations (Christophoul et al., 2002; Hermoza et al., 2005b; Roddaz et al., 2010). According to these authors, this Eocene marine incursion would come from both the Guyaquil Gulf and the Caribbean Sea (Fig. 15-B). Data from Colombia suggest that a late Eocene transgression flooded south-western Colombia, coming from the south through the Ecuadorian coast (Osorio et al., 2002; Santos et al., 2008). The presence of marine deposits in the Eastern Cordillera and the Central-Eastern Llanos Foothills is more difficult to explain and authors propose a possible corridor through the proto-Lower Magdalena Valley that connected the Caribbean Sea and the Central Llanos Foothills (Santos et al., 2008). In Ecuador and northern Peru, the Eocene shallow marine transgression is recorded by the deposits of Orteguzza and Pozo Formations (Fig. 2) as the result of the Western Cordillera loading (Roddaz et al., 2010). The southern limit of this marine incursion is not well-constrained but no Eocene deposits have been recognized in the southern Peruvian and Bolivian Amazonian basin (Fig. 2).

The nature of the Andean source (Eastern or Western Cordillera) for the sediments deposited within the Paleocene estuary also remains

unclear. Thermochronological evidences suggest that the first exhumation and/or deformation pulse in the eastern part of the Altiplano or in the Eastern Cordillera of Central Andes occurred in the late Eocene (Kontak et al., 1990; Barnes et al., 2006). Jaillard et al. (1993b) interpreted the absence of strata close to the K–Pg boundary in the Cusco basins as the consequence of an uplift of a proto-Eastern Cordillera occurring as early as the early to late Paleocene. However, provenance data suggest that the Paleocene estuarine sediments studied here are characterized by a contribution from a volcanic arc source. According to Mamani et al. (2010), the only active volcanic arc during the Paleocene was the Toquepala volcanic arc (91–45 Ma) located in the present-day Coastal/Western Cordillera. This suggests the absence of any significant proto-Eastern Cordillera relief capable of acting as a barrier to sediments originating from the Western Cordillera Arc. In conclusion, our data suggest that the Paleocene marine incursion could be related to proto-Western Cordillera loading. This orogenic loading can be related to a drastic change in convergence direction of the subduction from NE to ENE (Soler and Bonhomme, 1990) that might have provoked the major late Paleocene tectonic event formerly called Incaic 1 tectonic event (Noble et al., 1990; Sempere et al., 1997).

According to the data presented in this study and to literature review, at least two marine incursions occurred in the Amazonian foreland basin in early Paleogene times (Paleocene and Eocene, respectively). Both shallow marine incursions are mainly induced by Andean tectonic loading but they did not affect similar areas in the Amazonian foreland basins. Many studies (see Hoorn et al., 2010) have emphasized the role played by the Miocene long-lived Pebas megawetland system

Fig. 12 Thin section photographs from Facies C4, C5 and C6, sampled at MD-184. The number of each thin-section is indicated by “TS-no.”. They are located on the sedimentary Section 2 of Fig. 10. A), B), C) and D) correspond to thin-sections of alternated marl and limestone strata from Facies C4. E) and F) correspond to the stromatolitic Limestones of Facies C5. G), H), I) and J) correspond to the oyster limestones of Facies C6. Fi = Fish vertebra, Mi = Micritic pellets, Dru = Drusic cement, Ga = Gasteropod, Ph = Phylopod, Oy = Oyster, An = Annelid, Str = Stromatolith filaments.



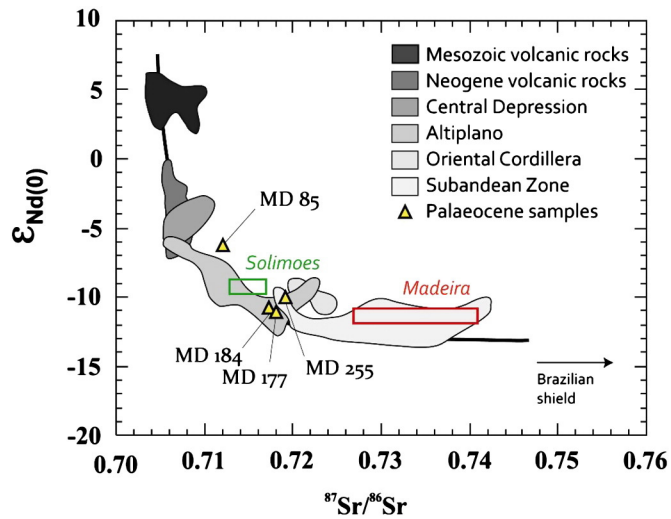


Fig. 13. $^{87}\text{Sr}/^{86}\text{Sr}$ versus $\epsilon\text{Nd}(0)$ diagram. Yellow triangles correspond to the Paleocene samples analyzed in this study. Note that they all plot within the melange hyperbole, indicating an Andean provenance. See text for details. (For interpretation of the references to color in this figure legend, the reader is referred to the web version of this article.)

in preventing in situ speciation and floristic and plants dispersal between the Andes and Amazonia for at least 6 Ma (Antonelli et al., 2009) and favoring evolutionary transition from marine to freshwater habitats of Neotropical fishes (Lundberg et al., 1998; Lovejoy et al., 2006, 2009). Recurrent Paleogene marine incursions in the Amazonian foreland basin associated with Andean uplift could have provoked biogeographical isolation and promoted allopatric speciation for terrestrial organisms.

7. Conclusions

Based on a multidisciplinary approach, this paper documents for the first time the presence of a tide-dominated shallow marine paleoenvironment during the Paleocene interval (Danian or Thanetian) in the Amazonian basin. In details, based on sedimentary facies analysis, organic geochemistry and fossil assemblages, three facies associations related to a tide-dominated estuary debouching into a shallow-marine bay or lagoon have been defined. Facies association A corresponds to

the sedimentary filling of a tide-influenced meandering channel formed in the fluvial–tidal transition zone. Facies association B is related to more distal tidal-flats, little channelized tidal inlets and saltmarsh deposits. Facies association C corresponds to a stressed shallow marine environment such as a bay or a lagoon.

The presence of these transgressive estuarine deposits overlying older continental facies is best explained by flexural tectonic subsidence in response to Andean tectonic loading. This is in agreement with the Nd–Sr isotopic provenance data that show an Andean provenance and hence the presence of an Andean relief during Danian or Thanetian times. The volcanic contribution recorded in the Nd–Sr isotopic compositions can be related to the Toquepala volcanic arc (91 to 45 Ma) located in the present-day Coastal/Western Cordillera. This suggests the absence of any significant proto-Eastern Cordillera relief that would have stopped the drainage and the sedimentary influxes from this Western Andean volcanic relief towards the Amazonian basin during Danian or Thanetian times. Consequently the data suggest that the Danian or Thanetian marine incursion can be related to the subsidence created in response to the proto-Western Cordillera loading. We suggest that this Paleocene transgression may come from the south and may be related to the Parana Sea. Finally, similar to Miocene marine incursions affecting the Pebas megawetland, Paleogene marine incursions in the Amazonian foreland basin associated with Andean uplift may have played a role in the dynamics of Neotropical paleobiodiversity in favoring biogeographical isolation and promoting allopatric speciation for terrestrial organisms.

Supplementary data to this article can be found online at <http://dx.doi.org/10.1016/j.palaeo.2014.09.027>.

Acknowledgments

We thank Denise Dorhout for analytical support at NIOZ. We are much indebted to Frank P. Wesselingh for mollusk taxonomic identification. The research leading to these results has received funding from the IRD (Institut de Recherche pour le Développement), the Institut Carnot (France), REPSOL Exploración and the European Research Council under the European Union's Seventh Framework Program (FP7/2007–2013)/ERC grant agreement no. [226600]. The authors wish to acknowledge the Editors of the Journal and the two anonymous reviewers for their critical comments.

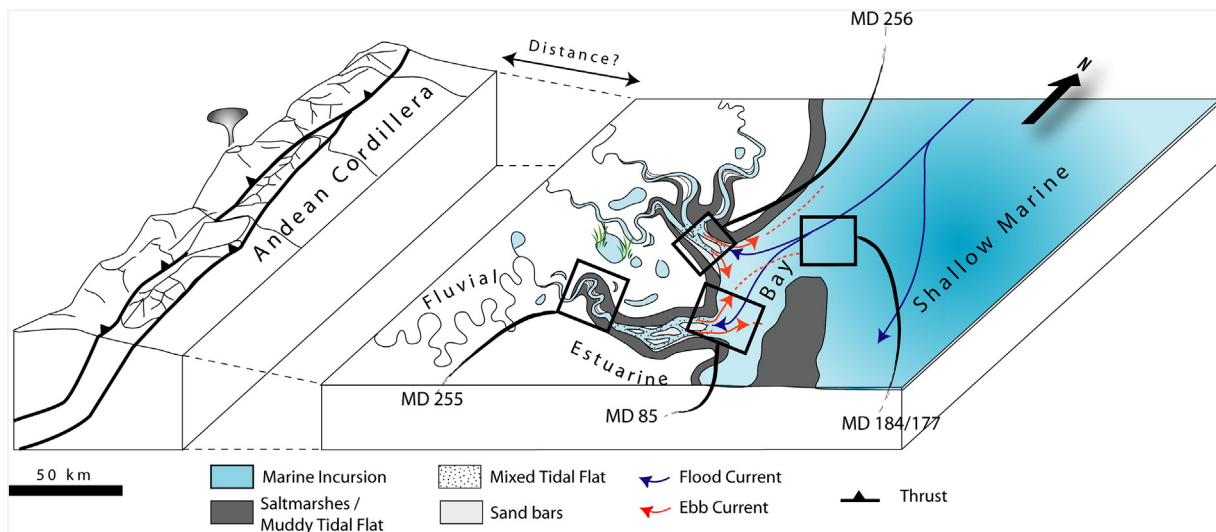


Fig. 14. Interpretative diagram for Paleocene times. Andean relief is active yet and produces sedimentary supply for the fluvial and then estuary system debouching in a shallow interior sea. Black rectangles correspond to the interpretative depositional context location of each outcrop: MD-255 corresponds to the fluvio–estuarine meandering transition zone in the proximal estuarine system; MD-256 corresponds to the inner (?) part of the estuary; MD-85 corresponds to the outer part of the estuary system and MD-184/177 corresponds to the most distal environment, also located around the outer part of the estuary system but more connected to a bay or calm confined shallow marine basin.

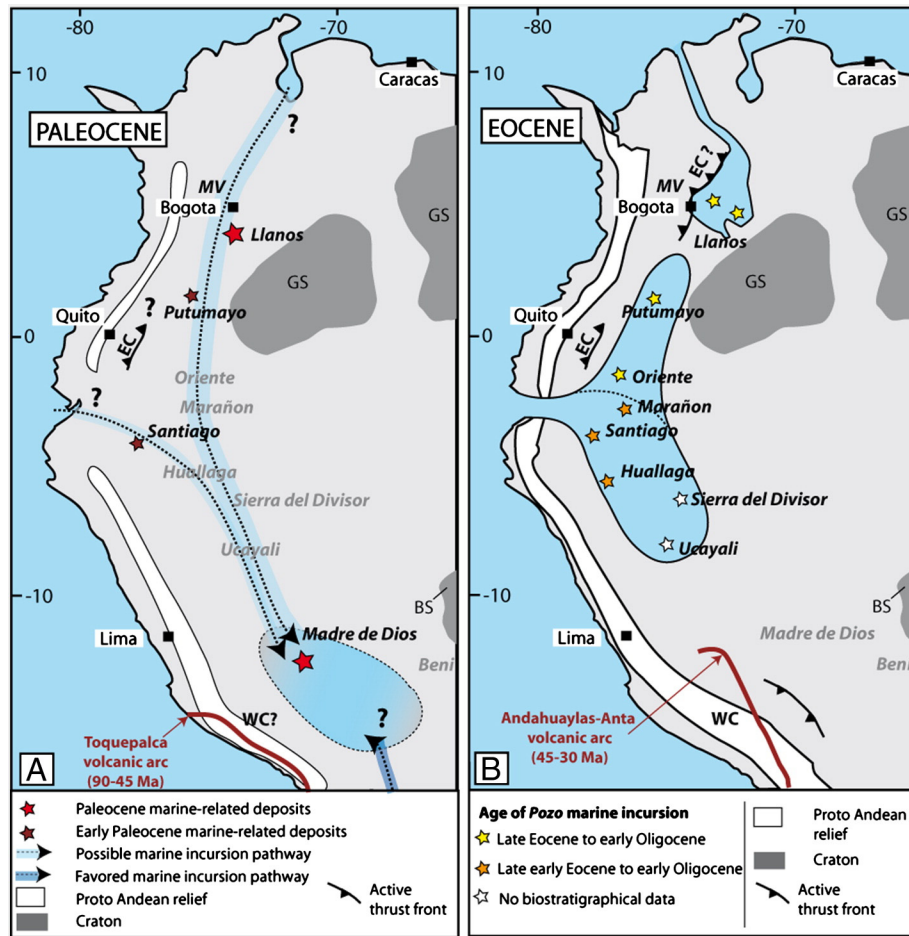


Fig. 15. Paleogeographical reconstructions for Paleogene times. A) Paleogeographic reconstruction of Paleocene times. The shallow marine sea described in this paper in the Amazonian foreland basin does not present clear connection with existing oceans. B) Paleogeographic reconstruction for Eocene times, related to Pozo shallow marine incursion. See text for details.

References

- Allen, J.R.L., 1970. A quantitative model of climbing ripples and their cross-laminated deposits. *Sedimentology* 14, 5–26.
- Antoine, P.-O., Marivaux, L., Croft, D.A., Billet, G., Ganerød, M., Jaramillo, C., Martin, T., Orliac, M.J., Tejada, J., Altamirano, A.J., 2012. Middle Eocene rodents from Peruvian Amazonia reveal the pattern and timing of caviomorph origins and biogeography. *Proc. R. Soc. B Biol. Sci.* 279, 1319–1326.
- Antoine, P.O., Roddaz, M., Bricchau, S., Tejada-Lara, J., Salas-Gismondi, R., Altamirano, A., Louterbach, M., Lambs, L., Otto, T., Brusset, S., 2013. Middle Miocene vertebrates from the Amazonian Madre de Dios Subandean Zone, Peru. *J. S. Am. Earth Sci.* 42, 91–102.
- Antoine, P.O., Billet, G., Salas-Gismondi, R., Tejada Lara, J., Baby, P., Brusset, S., Espurt, N., 2014n. A new *Carodnia* Simpson, 1935 (Mammalia, Xenungulata) from the early Eocene of Northwestern Peru and a phylogeny of xenungulates at species level. *J. Mamm. Evol.* (Submitted for publication).
- Antonelli, A., Nylander, J.A.A., Persson, C., Sanmartin, I., 2009. Tracing the Impact of the Andean Uplift on Neotropical Plant Evolution. *PNAS*.
- Armstrong, H.A., Brasier, M.D., 2005. Microfossil. In: Hart, M. (Ed.), *Geological Magazine*, 2nd ed. Blackwell Publishing, Malden, Oxford, Carlton.
- Ashley, G.M., Southard, J.B., Boothroyd, J.C., 1982. Deposition of climbing-ripple beds: a flume simulation. *Sedimentology* 29, 67–79.
- Aubry, M.-P., Thiry, M., Dupuis, C., Berggren, W., 2005. The Sparnacian deposits of the Paris Basin: a lithostratigraphic classification. *Stratigraphy* 2, 65–100.
- Barnes, J.B., Ehlers, T.A., McQuarrie, N., O'Sullivan, P.B., Pelletier, J.D., 2006. Eocene to recent variations in erosion across the central Andean fold-thrust belt, northern Bolivia: implications for plateau evolution. *Earth Planet. Sci. Lett.* 248, 118–133.
- Barragan, R., Geist, D., Hall, M., Larson, P., Kurz, M., 1998. Subduction controls on the compositions of lavas from the Ecuadorian Andes. *Earth Planet. Sci. Lett.* 154, 153–166.
- Basu, A.R., Sharma, M., Decelles, P.G., 1990. Nd, Sr-isotopic provenance and trace-element geochemistry of Amazonian foreland basin fluvial sands, Bolivia and Peru. Implications for ensialic Andean orogeny. *Earth Planet. Sci. Lett.* 100, 1–17.
- Bejarano, A., 1991. Caracterización y Evaluación de Parametros de Registros de Pozos en la Cuenca del Putumayo.
- Campbell, K.E., David, C., Romero-pittman, L., 2006. The Pan-Amazonian Ucayali Peneplain, late Neogene sedimentation in Amazonia, and the birth of the modern Amazon River system. *Palaeogeogr. Palaeoclimatol. Palaeoecol.* 239, 166–219.
- Cande, S.C., Kent, D.V., 1992. A new geomagnetic polarity time scale for the Late Cretaceous and Cenozoic. *J. Geophys. Res. Solid Earth* 97, 13917–13951.
- Cappetta, H., 2012. Chondrichthyes (Mesozoic and Cenozoic Elasmobranchii: teeth). In: Schultze, H.-P. (Ed.), *Handbook of Paleichthyology* (Munich (Pfeil)).
- Cappetta, H., Gayet, M., 2013. A new elasmobranch genus (Myliobatiformes, Dasyatoidea) from the Danian of Potosí (Bolivia). *Neues Jb. Geol. Paläontol. Abh.* 269, 285–290.
- Casero, P., 1997. Multidisciplinary Correlative Evidences for Polyphase Geological Evolution of the Foot-Hills of the Cordillera Oriental (Colombia).
- Catuneanu, O., 2004. Retroarc foreland systems—evolution through time. *J. Afr. Earth Sci.* 38, 225–242.
- Catuneanu, O., Beaumont, C., Waschbusch, P., 1997. Interplay of static loads and subduction dynamics in foreland basins: reciprocal stratigraphies and the “missing” peripheral bulge. *Geology* 25, 1087–1090.
- Catuneanu, O., Sweet, A.R., Miall, A.D., 1999. Concept and styles of reciprocal stratigraphies: Western Canada foreland system. *Terra Nova* (Oxford) 11, 1–8.
- Choi, K., 2010. Rhythmic Climbing-ripple cross-lamination in inclined heterolithic stratification (IHS) of a macrotidal estuarine channel, Gomso Bay, West Coast of Korea. *J. Sediment. Res.* 80, 550–561.
- Christophoul, F., Baby, P., Dávila, C., 2002. Stratigraphic responses to a major tectonic event in a foreland basin: the Ecuadorian Oriente Basin from Eocene to Oligocene times. *Tectonophysics* 345, 281–298.
- Cooper, M., Addison, F., Alvarez, R., Coral, M., Graham, R.H., Hayward, A., Howe, S., Martinez, J., Naar, J., Peñas, R., 1995. Basin development and tectonic history of the Llanos Basin, Eastern Cordillera, and middle Magdalena Valley, Colombia. *AAPG Bull.* 79, 1421–1442.
- Córdoba, F., Buchelli, F., Moros, J., Calderón, W., Guerrero, C., Kairuz, E., Magoon, L., 1997. Proyecto evaluación regional Cuenca del Putumayo—Definición de los sistemas petrolíferos. *ECOPETROL*, Bogotá.
- Dalrymple, R.W., 1984. Runoff microdeltas: a potential emergence indicator in cross-bedded sandstones. *J. Sediment. Res.* 54, 825–830.
- Dalrymple, R.W., Choi, K., 2007. Morphologic and facies trends through the fluvial–marine transition in tide-dominated depositional systems: a schematic framework for environmental and sequence-stratigraphic interpretation. *Earth Sci. Rev.* 81, 135–174.
- Dalrymple, R.W., Zaitlin, B.A., Boyd, R., 1992. Estuarine facies models: conceptual basis and stratigraphic implications. *J. Sediment. Res.* 62, 1130–1146.

- Dalrymple, R.W., Baker, E.K., Harris, P.T., Hughes, M.G., 2003. Sedimentology and stratigraphy of a tide-dominated, foreland-basin delta (Fly River, Papua New Guinea). In: Sidi, F.H., Nummedal, D., Imbert, P., Darman, H., Posamentier, H.W. (Eds.), *Tropical Deltas of Southeast Asia—Sedimentology, Stratigraphy, and Petrology*. SEPM, Special Publication, pp. 147–173.
- de Mowbray, T., Visser, M.J., 1984. Reactivation surfaces in subtidal channel deposits, Oosterschelde, Southwest Netherlands. *J. Sediment. Res.* 54, 811–824.
- DeCelles, P.G., Horton, B.K., 2003. Early to middle Tertiary foreland basin development and the history of Andean crustal shortening in Bolivia. *Geol. Soc. Am. Bull.* 115, 58–77.
- Dunham, R.J., 1962. Classification of carbonate rocks according to depositional texture. In: Ham, W.E. (Ed.), *Classifications of Carbonate Rocks — A Symposium*, pp. 108–121.
- Enay, R., 1990. *Paléontologie des invertébrés*. (Paris).
- Eriksson, K.A., Simpson, E.L., 2004. Precambrian tinalites: recognition and significance. In: Eriksson, P.G., Altermann, W., Nelson, D., Mueller, W., Cateneau, O., Strand, K. (Eds.), *Tempos and Events in Precambrian Time. Developments in Precambrian Geology*. Elsevier, Amsterdam, pp. 631–642.
- Eriksson, P.G., Condie, K.C., Tirsgaard, H., Mueller, W.U., Altermann, W., Miall, A.D., Aspler, L.B., Catuneanu, O., Chiarenzelli, J.R., 1998. Precambrian clastic sedimentation systems. *Sediment. Geol.* 120, 5–53.
- Faucher, B., Savoyat, E., 1973. Esquisse géologique des Andes de l'Equateur. *Rev. Géogr. Phys. Géol. Dyn.* 15, 115–142.
- Gayet, M., Sempere, T., Cappetta, H., Jaillard, E., Lévy, A., 1993. La présence de fossiles marins dans le Crétacé terminal des Andes centrales et ses conséquences paléogéographiques. *Palaeogeogr. Palaeoclimatol. Palaeoecol.* 102, 283–319.
- Gelfo, J.N., Sigé, B., 2011. A new didolodontid mammal from the late Paleocene–earliest Eocene of Laguna Umayo, Peru. *Acta Palaeontol. Pol.* 56, 665–678.
- Gelfo, J.N., Goin, F.J., Woodburne, M.O., Muizon, C.D., 2009. Biochronological relationships of the earliest South American Paleogene mammalian faunas. *Paleontology* 52, 251–269.
- Gérard, J.R.F., Bromley, R.G., 2008. *Ichnofabrics in Clastic Sediments: Application to Sedimentological and Core Studies. A Practical Guide* by Jean R.F. Gérard and Richard G. Bromley. Jean R.F. Gérard, Madrid.
- Gil, W.F., 2001. Evolution latérale de la déformation d'un front orogénique: exemples des bassins subandins entre 0° et 16°S. University Paul Sabatier, Toulouse.
- Gonella, C.A.C., Griffin, M., Cione, A., Cavalli, S.G., Aceñolaza, F.G., 2012. Paleontología de la Formación Yacoraita (Maastrichtiano–Daniano) en el ámbito de la Subcuenca de Tres Cruces, Cordillera Oriental de la provincia de Jujuy, Argentina.
- Gradstein, F., Kaminski, M., Berggren, W., 1988. Cenozoic foraminiferal biostratigraphy of the Central North Sea. *Abh. Geol. Bundesanst.* 41, 97–108.
- Gutierrez, M., 1982. Evaluación potencial petrolífera cuencas Huallaga, Ucayali y Madre de Dios. Zonación bioestratigráfica del intervalo Cretácico superior–Terciario inferior. *Petroperu, Internal Report*, Lima, p. 29.
- Haq, B.U., Hardenbol, J., Vail, P.R., 1987. Chronology of fluctuating sea levels since the Triassic. *Science* 235, 1156–1167.
- Hardenbol, J., Thierry, J., Farley, M.B., Jacquin, T., De Graciansky, P.C., Vail, P.R., 1998. Mesozoic–Cenozoic Sequence Chronostratigraphy of European Basins. 60 SEPM Special Publication, Tulsa, pp. 1–786.
- Herms, W., 2004. Dynamique tectono-sédimentaire et restauration séquentielle du retro-bassin d'avant-pays des Andes Centrales. Université Paul Sabatier, Toulouse, p. 196.
- Herms, W., Brusset, S., Baby, P., Gil, W., Roddaz, M., Guerrero, N., Bolaños, R., 2005b. The Huallaga foreland basin evolution: thrust propagation in a deltaic environment, northern Peruvian Andes. *J. S. Am. Earth Sci.* 19, 21–34.
- Hernandez, R.M., Jordan, T.E., Farjat, A.D., Echavarría, L., Idelman, B.D., Reynolds, J.H., 2005. Age, distribution, tectonics, and eustatic controls of the Paranaense and Caribbean marine transgressions in southern Bolivia and Argentina. *J. S. Am. Earth Sci.* 19, 495–512.
- Hoorn, C., Wesselingh, F.P., ter Steege, H., Bermudez, M.a., Mora, a., Sevink, J., Sanmartín, I., Sanchez-Meseguer, a., Anderson, C.L., Figueiredo, J.P., Jaramillo, C., Riff, D., Negri, F.R., Hooghiemstra, H., Lundberg, J., Stadler, T., Särkinen, T., Antonelli, A., 2010. Amazonia through time: Andean uplift, climate change, landscape evolution, and biodiversity. *Science (New York, N.Y.)* 330, 927–931.
- Hovikoski, J., Gingras, M., Räsänen, M., Rebata, L.A., Guerrero, J., Ranzi, A., Melo, J., Romero, L., del Prado, H.N., Jaimes, F., 2007. The nature of Miocene Amazonian epicontinental embayment: high-frequency shifts of the low-gradient coastline. *Geol. Soc. Am. Bull.* 119, 1506–1520.
- Hovikoski, J., Räsänen, M., Gingras, M., Ranzi, A., Melo, J., 2008. Tidal and seasonal controls in the formation of Late Miocene inclined heterolithic stratification deposits, western Amazonian foreland basin. *Sedimentology* 55, 499–530.
- Jackson, R.G., 1981. Sedimentology of muddy fine-grained channel deposits in meandering streams of the American Middle West. *J. Sediment. Res.* 51, 1169–1192.
- Jacobsen, S.B., Wasserburg, G.J., 1980. Sm–Nd isotopic evolution of chondrites. *Earth Planet. Sci. Lett.* 50, 139–155.
- Jaillard, E., 1993a. The Senonian to Palaeocene tectonic evolution of the Peruvian margin and its relationships with geodynamics. *Bull. Soc. Geol. Fr.* 164, 819–830.
- Jaillard, E., 1996. Cretaceous to early Paleogene tectonic evolution of the northern Central Andes (0–18°S) and its relations to geodynamics. *Tectonophysics* 259, 41–53.
- Jaillard, E., Carlotto, V., Cardenas, J., Chavez, R., Gil, W., 1993b. La "Nappe des Couches Rouges" de Cuzco (Sud du Pérou): mise en évidence stratigraphique, interprétations tectoniques et paléogéographiques. *C. R. Acad. Sci. Paris* 36, 379–386.
- Jaramillo, C.A., Dilcher, D.L., 2000. Microfloral diversity patterns of the late Paleocene–Eocene interval in Colombia, northern South America. *Geology* 28, 815–818.
- Jaramillo, C.A., Dilcher, D.L., 2001. Middle Paleogene palynology of Central Colombia, South America: a study of pollen and spores from tropical latitudes. *Palaeontogr. Abt. B* 258, 87–213.
- Jeffery, M.L., Poulsen, C.J., Ehlers, T.A., 2012. Impacts of Cenozoic global cooling, surface uplift, and an inland seaway on South American paleoclimate and precipitation $\delta^{18}O$. *Geol. Soc. Am. Bull.* 124, 335–351.
- Jopling, A.V., Walker, R.G., 1968. Morphology and origin of ripple-drift cross-lamination, with examples from the Pleistocene of Massachusetts. *J. Sediment. Res.* 38, 971–984.
- Kay, S.M., Coira, B., Viramonte, J., 1994. Young mafic back arc volcanic-rocks indicators of continental lithospheric delamination beneath the Argentine Puna plateau, Central Andes. *J. Geophys. Res. Solid Earth* 99, 24323–24339.
- Klein, G.D., 1970. Depositional and dispersal dynamics of intertidal sand bars. *J. Sediment. Res.* 40, 1095–1127.
- Kontak, D.J., Farrar, E., Clark, A.H., Archibald, D.A., 1990. Eocene tectono-thermal rejuvenation of an upper Paleozoic–lower Mesozoic terrane in the Cordillera de Carabaya, Puno, southeastern Peru, revealed by K–Ar and $^{40}Ar/^{39}Ar$ dating. *J. S. Am. Earth Sci.* 3, 231–246.
- Londoño, J., Lorenzo, J.M., Ramirez, V., 2012. Lithospheric flexure and related base-level stratigraphic cycles in continental foreland basins: an example from the Putumayo Basin, Northern Andes. In: Gao, D. (Ed.), *Tectonics and Sedimentation: Implications for Petroleum Systems*. AAPG Memoir, pp. 357–375.
- Lovejoy, N.R., Albert, J.S., Crampton, W.G.R., 2006. Miocene marine incursions and marine/freshwater transitions: evidence from Neotropical fishes. *J. S. Am. Earth Sci.* 21, 5–13.
- Lovejoy, N.R., Willis, S.C., Albert, J.S., 2009. Molecular Signatures of Neogene Biogeographical Events in the Amazon Fish Fauna. *Landscape and Species Evolution*. Wiley-Blackwell Publishing Ltd., Amazonia, pp. 405–417.
- Lundberg, J.G., Marshall, L.G., Guerrero, J., 1998. The stage of neotropical fish diversification: a history of tropical South American rivers. In: Malabarba, L.R., Reis, R.E., Vari, R.P., Lucena, Z.M., Lucena, C.A.S. (Eds.), *Phylogeny and Classification of Neotropical Fishes*. Edipucrs, Porto Alegre, p. 603.
- Mamani, M., Worner, G., Sempere, T., 2010. Geochemical variations in igneous rocks of the Central Andean orocline (13 degrees S to 18 degrees S): tracing crustal thickening and magma generation through time and space. *Geol. Soc. Am. Bull.* 122, 162–182.
- Marivaux, L., Salas-Gismondi, R., Tejada, J., Billet, G., Louterbach, M., Vink, J., Bailleul, J., Roddaz, M., Antoine, P.O., 2012. A platyrrhine talus from the early Miocene of Peru (Amazonian Madre de Dios Sub-Andean Zone). *J. Hum. Evol.* 63, 696–703.
- Marocco, R., Baudino, R., A., L., 1995. The intermontane Neogene continental basins of the Central Andes of Ecuador and Peru: sedimentological, tectonic and geodynamic implications. In: Tankard, A.J., R.S., Welsink, H.J. (Eds.), *Petroleum Basins of South America*. Am. Assoc. Pet. Geol. Mem., pp. 597–613.
- Marshall, L.G., Sempere, T., Butler, R.F., 1997. Chronostratigraphy of the mammal-bearing Paleocene of South America. *J. S. Am. Earth Sci.* 10, 49–70.
- Martin-Gomboj, N., Winkler, W., 2008. Recycling of proterozoic crust in the andean amazon foreland of Ecuador: implications for orogenic development of the Northern Andes. *Terra Nova* 20, 22–31.
- Mazumder, R., Arima, M., 2005. Tidal rhythmites and their implications. *Earth Sci. Rev.* 69, 79–95.
- Meyers, P.A., 1997. Organic geochemical proxies of paleoceanographic, paleolimnologic, and paleoclimatic processes. *Org. Geochem.* 27, 213–250.
- Miall, A.D., 1996. *The Geology of Fluvial Deposits: Sedimentary Facies, Basin Analysis and Petroleum Geology*. Springer-Verlag Inc. Berlin.
- Mitrovica, J., Beaumont, C., Jarvis, G., 1989. Tilting of continental interiors by the dynamical effects of subduction. *Tectonics* 8, 1079–1094.
- Morsi, A.-M.M., Speijer, R.P., Stassen, P., Steurbaut, E., 2011. Shallow marine ostracode turnover in response to environmental change during the Paleocene–Eocene thermal maximum in northwest Tunisia. *J. Afr. Earth Sci.* 59, 243–268.
- Mpodozis, C., Allmendinger, R.W., 1993. Extensional tectonics, Cretaceous Andes, northern Chile (27°S). *Geol. Soc. Am. Bull.* 105, 1462–1477.
- Musacchio, E.A., 1990. Non-marine Cretaceous Ostracods from Argentina and their Palaeobiogeographical Relationships, Ostracoda and Global Events. Springer, pp. 557–569.
- Naeser, C.W., Crochet, J., Jaillard, E., Laubacher, G., Mourier, T., Sigé, B., 1991. Tertiary faunal-track ages from the Bagua syncline (northern Peru): stratigraphic and tectonic implications. *J. S. Am. Earth Sci.* 4, 61–71.
- Nio, S.D., Yang, C.S., 1991. Diagnostic attributes of clastic tidal deposits: a review. In: Smith, D.G., Reinson, G.E., Zeitlin, B.A., Rahmani, R.A. (Eds.), *Clastic Tidal Sedimentology*. Canadian Society of Petroleum Geologists, pp. 3–28.
- Noble, D.C., McKee, E.H., Mourier, T., Mégar, F., 1990. Cenozoic stratigraphy, magmatic activity, compressive deformation, and uplift in Northern Peru. *Geol. Soc. Am. Bull.* 102, 1105–1113.
- Osorio, C., Michoux, D., Tellez, G., 2002. Stratigraphy of the Tertiary sequences — Upper Magdalena and the Putumayo basins, a different point of view for hydrocarbon exploration. *Memorias de la Segunda Convención técnica de la Asociación Colombiana de Geólogos y Geofísicos del Petróleo*, Bogotá, Colombia. p. 10.
- Page, K.J., Nanson, G.C., Frazier, P.S., 2003. Floodplain formation and sediment stratigraphy resulting from oblique accretion on the Murrumbidgee River, Australia. *J. Sediment. Res.* 73, 5–14.
- Parra, M., Mora, A., Jaramillo, C., Strecker, M.R., Sobel, E.R., Quiroz, L., Rueda, M., Torres, V., 2009. Orogenic wedge advance in the northern Andes: evidence from the Oligocene–Miocene sedimentary record of the Medina Basin, Eastern Cordillera, Colombia. *Geol. Soc. Am. Bull.* 121 (5–6), 780–800.
- Peters, K.E., Cassa, M.R., 1994. Applied source rock geochemistry. *Mem. Am. Assoc. Pet. Geol.* 93–93.
- Pinto, L., 2003. Traçage de l'érosion Cénozoïque des Andes Centrales à l'aide de la minéralogie et de la géochimie des sédiments (Nord du Chili et Nord-Ouest de la Bolivie). Université Paul Sabatier, Toulouse.
- Poyato-Ariza, F.J., Wenz, S., 2002. A new insight into pycnodontiform fishes. *Geodiversitas* 24, 139–248.
- Pysklywec, R., Mitrovica, J., 2000. Mantle flow mechanisms of epeirogeny and their possible role in the evolution of the Western Canada Sedimentary Basin. *Can. J. Earth Sci.* 37, 1535–1548.

- Roddaz, M., Viers, J., Brusset, S., Baby, P., Hérail, G., 2005a. Sediment provenances and drainage evolution of the Neogene Amazonian foreland basin. *Earth Planet. Sci. Lett.* 239, 57–78.
- Roddaz, M., Hermoza, W., Mora, A., Baby, P., Parra, M., Christophoul, F., Brusset, S., Espurt, N., 2010. Cenozoic sedimentary evolution of the Amazonian foreland basin system. In: Blackwell (Ed.), *Amazonia, Landscape and Species Evolution*, pp. 61–88.
- Roddaz, M., Christophoul, F., Zambrano, J.D.B., Soula, J.C., Baby, P., 2012. Provenance of late Oligocene to quaternary sediments of the Ecuadorian Amazonian foreland basin as inferred from major and trace element geochemistry and Nd–Sr isotopic composition. *J. S. Am. Earth Sci.* 37, 136–153.
- Rogers, G., Hawkesworth, C.J., 1989. A geochemical traverse across the North Chilean Andes: evidence for crust generation from the mantle wedge. *Earth Planet. Sci. Lett.* 91, 271–285.
- Ruiz, G.M.H., Seward, D., Winkler, W., 2004. Detrital thermochronology – a new perspective on hinterland tectonics, an example from the Andean Amazon Basin, Ecuador. *Basin Res.* 16, 413–430.
- Ruiz, G.M.H., Seward, D., Winkler, W., 2007. Evolution of the Amazon Basin in Ecuador with Special Reference to Hinterland Tectonics: Data from Zircon Fission-Track and Heavy Mineral Analysis. pp. 907–934.
- Santos, C., Jaramillo, C., Bayona, G., Rueda, M., Torres, V., 2008. Late Eocene marine incursion in north-western South America. *Palaeogeogr. Palaeoclimatol. Palaeoecol.* 264, 140–146.
- Sempere, T., Butler, R.F., Richards, D.R., Marshall, L.G., Sharp, W., Swisher, C.C., 1997. Stratigraphy and chronology of upper Cretaceous lower Paleogene strata in Bolivia and northwest Argentina. *Geol. Soc. Am. Bull.* 109, 709–727.
- Sigé, B., Sempere, T., Butler, Robert F., Marshall, Larry G., Crochet, J.-Y., 2004. Age and stratigraphic reassessment of the fossil-bearing Laguna Umayo red mudstone unit, SE Peru, from regional stratigraphy, fossil record, and paleomagnetism. *Geobios* 37, 771–794.
- Soler, P., Bonhomme, M.G., 1990. Relation of magmatic activity to plate dynamics In central Peru from Late Cretaceous to present. In: Kay, S.M., Rapela, C.W. (Eds.), *Plutonism from Antarctica to Alaska: Boulder, Colorado. Geological Society of America Special Paper*.
- Steurbaud, E., Magioncalda, R., Dupuis, C., Van Simaëys, S., Roche, E., Roche, M., 2003. Palynology, paleoenvironments, and organic carbon isotope evolution in lagoonal Paleocene–Eocene boundary settings in North Belgium. *Spec. Pap. Geol. Soc. Am.* 291–318.
- Tessier, B., 1996. River–Ocean Interaction Zone: a Facies Model with Climbing Ripple Bedding. In: Romania, N.I.o.M.G.a.G.-e.o (Ed.), *GEO-ECO-MARINA 2. Workshop on “Fluvial–Marine Interactions”*, Malnas, Romania.
- Tyson, R.V., 1995. *Sedimentary Organic Matter: Organic Facies and Palynofacies*. Springer.
- Valchev, B., 2007. Representatives of Family Eggerellidae Cushman, 1937 from the Paleocene of the Coastal Part of East Stara Planina. *Rev. Bulg. Geol. Soc.* 68, 36–40.
- Vandenbergh, N., Hilgen, F., Speijer, R., 2012. The Paleogene Period. *The Geologic Time Scale 2012*. pp. 855–921.
- Viers, J., Roddaz, M., Filizola, N., Guyot, J.L., Sondag, F., Brunet, P., Zouiten, C., Boucayrand, C., Martin, F., Boaventura, G.R., 2008. Seasonal and provenance controls on Nd–Sr isotopic compositions of Amazon rivers suspended sediments and implications for Nd and Sr fluxes exported to the Atlantic Ocean. *Earth Planet. Sci. Lett.* 274, 511–523.
- Wattinne, A., 2004. Évolution d'un environnement carbonate lacustre à bioconstructions, en Limagne bourbonnaise (Oligo-Miocène, Massif Central, France). Thèse du Muséum National d'Histoire Naturelle, Paris p. 195.
- Woodburne, M.O., Goin, F.J., Bond, M., Carlini, A.A., Gelfo, J.N., López, G.M., Iglesias, A., Zimicz, A.N., 2014. Paleogene land mammal faunas of South America; a response to global climatic changes and indigenous floral diversity. *J. Mamm. Evol.* 21, 1–73.